Journal of Non-Crystalline Solids: X 17 (2023) 100161

Contents lists available at ScienceDirect

Journal of Non-Crystalline Solids: X

journal homepage: www.sciencedirect.com/journal/journal-of-non-crystalline-solids-x

Effect of modifier cation size on the structure, properties and nickel speciation in BK7 type alkali borosilicate glasses

Brian Topper [a,b], Lucas Greiner [a], Randall E. Youngman [c], Darren Stohr [a], Efstratios I. Kamitsos [d], Doris Möncke [a,*]

[a] Inamori School of Engineering at the New York State College of Ceramics, Alfred University, 1 Saxon Drive, Alfred, NY 14802, USA
[b] Department of Physics & Astronomy and Center for High Technology Materials, University of New Mexico, Albuquerque, NM 87131, USA
[c] Science and Technology Division, Corning Incorporated, Corning, New York 14831, USA
[d] Theoretical and Physical Chemistry Institute, National Hellenic Research Foundation, 48 Vassileos Constantinou Avenue, 11635 Athens, Greece

ARTICLE INFO

Keywords:
Alkali borosilicate glasses
Divalent and trivalent nickel ions in various coordination environments
Raman and infrared spectroscopy
Connectivity of borate and silicate groups
Packing density
Structure property correlation

ABSTRACT

Alkali-borosilicate glasses $16M_2O–10B_2O_3–74SiO_2$ were studied for M = Li to Cs. ^{11}B NMR showed 57% four-fold coordinated boron for Li, but 88 to 97% for M = Na to Cs. The fraction of neutral borate triangles decreases from Na to Cs. Vibrational spectroscopy shows significant non-bridging oxygen on silicate species for Li, decreasing to a low level from Na to Cs. The glass transition temperature is highest for M = Cs and correlates with increasing network connectivity. Sub-liquidus phase separation and homonuclear bonding was observed for M = Li, while M = Na to Cs show good linking of silicate with borate tetrahedra. Raman spectroscopy reveals a maximum of danburite rings for M = K, the glass with the highest packing density. Glasses doped with Ni_2O_3 changed color from yellow (Li) to purple (Na), to blue in samples of higher optical basicity (K, Rb, Cs). Tetrahedral Ni^{2+} likely coexists with trivalent nickel, Ni^{3+}, in blue glasses, while higher coordinated Ni^{2+} prevails in the yellow Li-sample.

1. Introduction

Alkali borosilicate glasses present a technically important glass system. The chemical composition affects the borate-silicate connectivity as well as the isomerization equilibrium between triangular and tetrahedral metaborate units, $BØ_2O^- \rightleftharpoons [BØ_4]^-$ (Ø = bridging oxygen, bO; O = non-bridging oxygen, nbO) [1–6]. Many alkali borosilicate glasses are notorious for sub-liquidus amorphous phase separation. Even sodium borosilicate compositions with enough alkali oxide to fall outside the compositional range prone to phase separation, might show preferential bonding between the various silicate and borate species [7,8]. Furthermore, the type of alkali modifier can impact the tendency for phase separation [7,9], as does the thermal history of the glass [10,11]. Additives like Al_2O_3 might prevent phase separation in glasses such as Duran® or Pyrex® [6,12,13], while MnO might induce phase separation in low alkali borosilicate glasses [14].

The presence of tetrahedral borate units with four bridging oxygen atoms, as opposed to the formation of triangular borate units with negatively charged non-bridging oxygen atoms (nbO), increases the connectivity of the covalent network, and this results in anomalous property behavior of borate as well as borosilicate glasses. This phenomenon is commonly referred to as the *boron oxide anomaly* [8,15]. The change in boron coordination makes borate and borosilicate glasses exciting to study, as does the plethora of superstructural units that are well known for borate systems [8,16,17], and to a certain degree in borosilicate glasses [5,18–21]. Here, ring units with a different number of silicate and borate tetrahedra can be distinguished by their characteristic ring breathing modes in the Raman spectra [4,5,18,19,22,23].

Spectroscopic techniques that directly probe the glass structure include NMR [1,13,19,20,24] and vibrational spectroscopies [1,4,5,14,17,18,25,26]. Probe ions such as transition metal or rare-earth elements are additional useful tools in structural studies [1,10,14,25,27,28], and have been used early on in glass science [29–38]. These studies rely on ions that are either absorbing in the visible-NIR wavelength region or show photoluminescence, and which can be introduced in trace amounts to the glass matrix without the dopant impacting the network structure. These ions will have their local environment dictated by the surrounding bulk structure and if, such as

* Corresponding author.
E-mail address: moncke@alfred.edu (D. Möncke).

https://doi.org/10.1016/j.nocx.2023.100161
Received 7 September 2022; Received in revised form 1 February 2023; Accepted 2 February 2023
Available online 4 February 2023

transition metal ions, they seek out high basicity sites, this permits the detection of structures like nbO's at very low levels [28]. Or they can probe the glass homogeneity by early detection of clustering as precursor of phase separation, via EPR or fluorescence spectroscopy [14,25,28]. Ni^{2+} and Co^{2+} have been used historically for their color change related to nbO formation [30,36,38] and the clustering of heavy dopants is also useful for SEM studies of phase separation [27,28]. For Ni^{2+} and Co^{2+} the divalent state was long the only accepted oxidation state, based by Bamford's declaration that trivalent nickel ions are not stable in glasses [39]. As far as we know, this concept of the preeminence of Ni^{2+} has never been questioned by any glass researcher [40]. Partially, this is related to the high third ionization energy of Ni^{3+} and the general instability of Ni^{3+} or Ni^{4+} complexes [41]. However, for the very similar cobalt ion, Dietzel [42] showed the presence of Co^{3+} in high basicity glasses, which was later replicated by Möncke and Ehrt [43]. Furthermore, these authors showed that photo-oxidation of divalent to trivalent nickel does occur for glasses of higher optical basicity doped with tetrahedral Ni^{2+}, such as window glass or the BK7, the technical sodium borosilicate glass of the current study and sometimes referred to as NBS1 in the literature [43,44].

Thus, to better understand the effect of the type of modifier cation on the structure and properties of a glass with a constant modifier to network former ratio, the glass series $16M_2O$–$10B_2O_3$–$74SiO_2$ (in mol%) was studied, where M is varied from Li to Cs. Sub-liquidus phase separation will be discussed first in more detail on the example of the lithium glass (section 3.1), which showed opaque regions even when quenched rapidly. This is followed by a section on basic glass properties (section 3.2). With larger cations, the polarizability, refractive index, and optical basicity of glass is expected to increase, which in turn should impact nickel speciation in the glasses (section 3.3). Less clear is the impact of the alkali cations regarding network modifications. In general, the distribution of non-bridging oxygen can vary between silicate and borate groups and depends, for example, on the metaborate equilibrium ($B\emptyset_2O^- \rightleftharpoons [B\emptyset_4]^-$), and the disproportionation of silicate species ($2Q^3 \rightleftharpoons Q^2 + Q^4$). Finally, the interconnectivity of silicate and borate units might vary in terms of preferential bonding or even phase separation. To investigate these issues, we employ NMR (section 3.4), IR (section 3.5) and Raman (section 3.6) spectroscopies. Finally, we correlate the observed structural changes with the glass properties (section 3.7).

2. Experimental

Sample names relate to the specific alkali oxide used in each borosilicate as MBS, with M = Li, Na, K, Rb or Cs. The two mixed glasses LNBS and RCBS contain 8 mol% of both Li_2O and Na_2O, or Rb_2O and Cs_2O, see also Table 1.

2.1. Materials

2.1.1. Glass preparation

The glasses of this study follow the molar composition 16 M_2O – 10 B_2O_3–74 SiO_2 with M = Li, Na, K, Rb, and Cs. Nickel oxide was doped additively as 0.1 mol% Ni_2O_3. Mixed glasses with 50:50 alkali contributions (16 M_2O = 8 Li_2O + 8 Na_2O and 8 Rb_2O + 8 Cs_2O) were also prepared to provide better insights into the evolution of certain spectral features. Glasses were made from high purity ingredients (all >99%) using alkali carbonates, H_3BO_3, SiO_2, and Ni_2O_3. Several series, doped and undoped, were melted from exploratory 8 g to larger 50 g batches, using Pt crucibles covered with a lid. All data and spectra displayed are from these large melt quantities, though we see a high reproducibility, even for the two earlier-made melts using SiO_2 crucibles. Small, 8-g, batches mixed with a pestle and mortar were melted at 1450–1550 °C for 30 min, the exact temperature depended on the composition. The melting time was increased to 120 min for the larger 50 g batches. When the viscosity permitted, melts were initially quenched between two metal plates. Rapid quenching was essential for the lithium borosilicate system to reduce sub-liquidus phase separation (see discussion in section 3.1). All other glasses were annealed at T_g – 20 °C for 30 min. When not otherwise mentioned, e.g., in section 3.1 when the opaque phases of LBS are studied, spectra and property data of quenched, glassy LBS are used.

2.1.2. Reference materials

Crystalline Danburite ($CaB_2Si_2O_8$ from Charcas, San Luis Potosi, Mexico, M29016) and crystalline Reedmergnerite ($NaBSi_3O_8$ from Tienshan Mountains, Tajikistan, M45676) were used as Raman references. Both samples were made available by the Royal Ontario Museum, M29016 and M45676 are the respective reference numbers.

2.2. Glass characterization

2.2.1. Physical properties

Density measurements were performed by the Archimedes method using high purity kerosene as immersion fluid. Each glass was measured at room temperature, 25 °C, at least 3 times and the resulting uncertainties were found to be less than ±0.01 g/cm^3 (even when overestimating the instrumental errors). The index of refraction was determined with an Abbe refractometer using the sodium D line at 589.3 nm. Each glass was measured at least three times and the resulting

Table 1
Physical properties of $16M_2O$ $10B_2O_3$–$74SiO_2$ glasses with M = Li, Na, K, Rb and Cs, undoped and additively doped with 0.1 mol% Ni_2O_3. Coordination number (CN) as discussed in the text, respective cation radii (r) and cation field strength (FS), transition temperature (T_g), density (ρ), molar volume (V_m), packing density (C_g), refractive index (n_D), oxygen polarizability (α_O^{2-}), theoretical and experimental optical basicity (Λ_{th} and Λ_n), fraction of four-fold coordinated boron (N_4), vibration frequency of the M cation against its site ($\tilde{\nu}_{M\text{-}O}$), and force constant of the M cation – site interactions ($F_{M\text{-}O}$).

	LBS	*LNBS*	NBS	KBS	RBS	*RCBS*	CBS
M_2O or $(M_2O + M'_2O)/2$	Li_2O	*$Li_2O + Na_2O$*	Na_2O	K_2O	Rb_2O	*$Rb_2O + Cs_2O$*	Cs_2O
CN (see text)	4	–	6	8	10	–	12
Cation radius, r (Å) [45]	0.590	–	1.02	1.51	1.66	–	1.88
FS = Z/r^2 (Å^{-2})	2.87		0.96	0.44	0.36		0.28
T_g (°C) ± 1	490	*495*	571	637	668	*666*	677
ρ (g/cm^3) ± 0.01	2.28	*2.36*	2.42	2.42	2.71	*2.76*	2.84
V_m (cm^3/mol)	24.7	*24.9*	25.4	27.5	30.0	*32.2*	34.0
Packing density, C_g	0.496	*0.505*	0.510	0.542	0.525	*0.513*	0.513
n_D ± 0.0002	1.5001	*1.5076*	1.5092	1.5114	1.5152	*1.5055*	1.5218
α_O^{2-} (Å^3)	1.7	*1.50*	1.52	1.57	1.66	*1.70*	1.91
Λ_{th}	0.497	*0.508*	0.520	0.537	0.544	*0.549*	0.553
Λ_n	0.485	*0.502*	0.517	0.553	0.617	*0.644*	0.796
N_4 (NMR)	0.57	*0.70*	0.88	0.92	0.93	*0.97*	0.97
IR, $\tilde{\nu}_{M\text{-}O}$ (cm^{-1})	294#	*n.a.*	171	138	99	*n.a.*	84#
$F_{M\text{-}O}$ (10^4 dyn/cm)	1.452#	*n.a.*	1.152	0.987	0.675	*n.a.*	0.536#

Approximate extrapolated values.

uncertainties were ± 0.0002 or less. Blue colored samples could not be measured at 589 nm. The glass transition temperatures were measured by differential scanning calorimetry (DSC) in platinum pans, using a TA Instruments SDT600 DSC TGA over the temperature range from 20 to 1000 °C with a heating rate of 20 °C/min. The reported T_g values were determined using the intercept technique and represent the onset of the glass transition event.

2.2.2. XRD and SEM measurements

Only the LBS samples showed turbidity which could be reduced by fast quenching, but which could not totally be eliminated (see Fig. 1). Thus, X-ray diffraction (XRD) was used to confirm the amorphous nature of the LBS sample. A Bruker D2 Phaser XRD was utilized, equipped with a Cu X-ray source and LynxEye high speed PSD detector. Measurements were performed at 30 kV and 10 mA, measuring bulk samples from 10 to 70°2θ in 0.03-degree increments with a 1 s scan time.

Scanning Electron Microscopy (SEM) was used to better understand the cause of the observed opacification for LBS. A JOEL JSM7800F SEM was employed to image the surface of a ground and polished, annealed LBS glass sample which was etched in nitric acid (trace metal grade 67–70%) for <1 min to create a surface profile by dissolution of the chemically less stable lithium borate rich phase [8]. A thin coating of Au was deposited on the etched exterior to mitigate charging on the sample surface. SEM images were taken of the samples using both backscattering and secondary electron imaging modes.

2.2.3. Spectroscopy

Optical spectroscopy was performed in transmission mode on optically polished sample plates, using a Perkin Elmer Lambda 950 with a 2 nm resolution over the range 200–3000 nm. The measured spectra were normalized to the thickness of the sample, which ranged between 2 and 4 mm.

Infrared spectra were taken on a Bruker Invenio R FTIR Dry Air Purge spectrometer. Measurements were made in reflectance mode at an 11° angle of incidence. A single continuous wide range scan measured R(ν) over the range 30–6000 cm^{-1}. Background measurements were taken from the average of 500 scans on a gold mirror. Sample measurements were taken using the average of 1000 scans on polished glass samples. After extrapolation of R(ν) to frequency values of zero and infinity, the reflectance spectra were used to calculate the real and imaginary parts of the complex refractive index using the Kramers-Kronig transformation function in the *OPUS* software [46]. The absorption coefficient spectra $\alpha(\nu)$ were calculated using the extinction coefficient k(ν) by $\alpha(\nu) = 4\,\pi\,\nu\,k(\nu)$. The absorption coefficient spectra were normalized to the area over the range 0–1600 cm^{-1}.

Raman spectra were measured in backscattering configuration on a WITech Alpha300 using a 488 nm excitation source and a 50× objective. The spectra were obtained by averaging 100–200 accumulations using a one second integration time. The Raman spectra were normalized to the area in the 100–1550 cm^{-1} interval. The crystalline reference borosilicate materials were min-max normalized and scaled to facilitate side by side comparison between the broad band characteristics of glasses with the sharp bands of the borosilicate minerals.

^{11}B magic-angle spinning (MAS) NMR measurements were conducted on an Agilent DD2 spectrometer in conjunction with a 16.4 T Agilent 700/54 Premium Shielded superconducting magnet, resulting in a ^{11}B resonance frequency of 224.52 MHz. Glasses were powdered with an agate mortar and pestle, and immediately loaded into a 3.2 mm zirconia rotor for computer-controlled sample spinning at 20.0 kHz using dry, compressed nitrogen. MAS NMR data were acquired under direct polarization, using a combination of a short radio-frequency pulse width of 0.6 μs (π/12 tip angle), a 2 s recycle delay and averaging of nominally 1000 acquisitions. ^{11}B MAS NMR data were processed in VnmrJ software (Agilent) without apodization and frequency referenced to a secondary shift standard of aqueous boric acid at 19.6 ppm relative to BF_3-etherate. NMR spectra were fitted using DMFit [47], with 2nd-order quadrupolar lineshapes (Q_MAS) for BO_3 resonances and mixed Gaussian/Lorentzian functions for BO_4 resonances. Multiple BO_3 resonances were required to adequately reproduce the trigonal boron signal. To accurately determine the fraction of boron in four-fold coordination (N_4), a small correction to the BO_4 peak area was made by fitting the first set of satellite transition spinning sidebands to estimate the contribution from the hidden sideband under the central transition peak near 0 ppm [48].

Electron paramagnetic resonance (EPR) spectra were recorded using a continuous-wave X-Band EPR spectrometer (Bruker Xenon). Crushed glass samples of approximately 0.161 g were place into standard 5 mm NMR tubes for measurement at room temperature and for some spectra, at liquid nitrogen temperature. Data were collected with a 2.056 mW microwave power, a modulation amplitude of 4 G and a microwave modulation frequency of 100 kHz. Each spectrum was the average of 10 scans.

2.2.4. Cation field strength and optical basicity

The field strength and optical basicity values were calculated from the nominal composition and literature values for the ionic radii and oxide basicities, respectively. Values were also obtained experimentally from the oxygen polarizability as derived from density and refractive index measurements. Equations and more details on the used values are given in section 3.2.1.

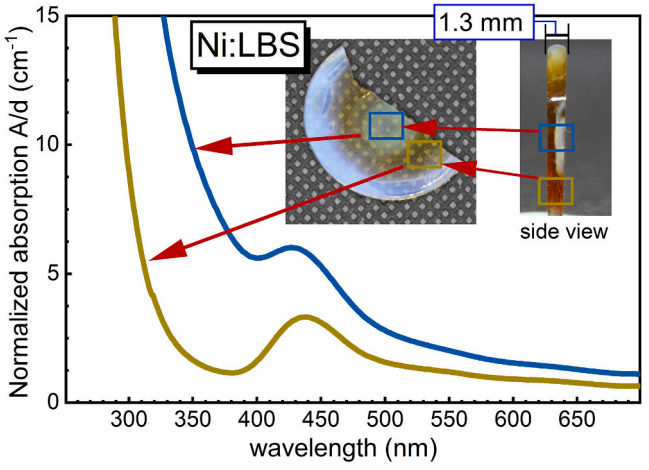

Fig. 1. Thickness normalized optical spectra of quenched nickel containing LBS glass. The inset shows the top and side view of the sample, indicating the respective probed regions.

3. Results and discussion

We will briefly discuss the observed trends in the appearance, glass properties, basicity, and color as well as nickel speciation, before discussing structural changes as deduced from ^{11}B NMR and vibrational spectroscopy. Finally, we will discuss structure-property correlations for the various modifier cations.

XRF and SEM-EDS could not reliably quantify the lighter elements, Li, B, or oxygen. However, the ratio of heavier elements (Na, K, Rb and Cs) versus Si was reproducible in samples melted at different times. No significant surplus of Si:M was seen in the sample melted in silica compared to samples melted in Pt crucibles. The NBS sample agreed in composition, properties (density, T_g, refractive index), and spectra with older NBS melts for which quantitative analysis was available [49]. This reproducibility of properties across melts of different size and duration of synthesis provides confidence that evaporation losses are low. In general, all samples from different melting campaigns show comparable properties and spectral features, even though some variations are evident for Raman spectra taken from a quenched surface compared to

spectra taken from well annealed bulk samples.

3.1. Phase separation of LBS

The lithium glass samples did not form a homogenous, clear, transparent glass, but showed significant opacification. Fig. 1 shows a rapidly quenched, partially opaque sample and the ensuing optical spectra taken from a clear and a semi-opaque region. For the study of the devitrified region, tempered, fully opaque samples were further studied by X-ray diffraction (XRD) and scanning electron microscopy (SEM).

In Fig. 1, the yellow optical spectrum corresponds to the clear glassy section, while the blue spectrum shows absorption losses at short wavelengths due to scattering in the semi-opaque sample. Annealed LBS samples turn fully opaque but even these samples are X-ray amorphous, as evident from Fig. 2.

Fast quenching partially reduced the opacity of the LBS samples, while heat treatment above T_g intensifies opacification. No crystalline inclusions were observed under the SEM, though spherical phases can be identified by backscattering and secondary electron imaging, as shown in Fig. 3. While our SEM-EDS is not able to quantify very light elements such as B or Li, light colored spheres of lower density are evident in a darker matrix of higher density using backscattering electron imaging, which does depend on the atomic number [50]. Considering the lighter molar mass of B and Li compared to heavier Si, and in analogy to sodium borosilicate glasses [7,8,14,28], the image indicates the formation of lithium borate rich droplets in a silica rich matrix. The stated compositional variations must be seen relative to the nominal composition of a homogenous glass and the degree of phase separation will also depend on the temperature and time of thermal treatment.

Fig. 4 depicts the range of phase separation for the ternary alkali-borosilicate systems as collected by Mazurin et al. [7]. The range of immiscibility depends not only on the composition and temperature, but also on the field strength of the modifier cation [24]. For the MBS composition, only the lithium containing glass LBS falls inside the range of phase separation, while the sodium containing sample is just outside the compositional region that shows phase separation for the sodium system. NBS coincides in its composition with the technical glass BK7, a common glass in optical applications. Contrary to low sodium borosilicate glasses like Duran® or Pyrex®, where alumina addition is crucial to prevent phase separation, NBS or BK7 do not need such special considerations to achieve homogenous glasses. Sastry and Hummel [51] studied the LBS system in the 1960's, describing sub-liquidus phase separation and the effect of the quenching rate and secondary heat treatment in the lithium borosilicate glass system. The authors distinguish a phase that is very soluble in aqueous solution, assumed to be lithium borate rich, and a remaining phase with a coefficient of thermal expansion that is close to silica. Ehrt et al. studied the distribution of cobalt and iron ions in a phase separated borosilicate glass matrix and reported that the transition metal ions preferentially accumulate in the sodium borate rich matrix [28,52], a finding that also applied to manganese ions [14]. However, the concentration of 0.1 mol% Ni_2O_3 was too small to accurately measure by SEM-EDS any distribution differences between the two phases.

Visible sub-liquidus phase separation of two amorphous phases with

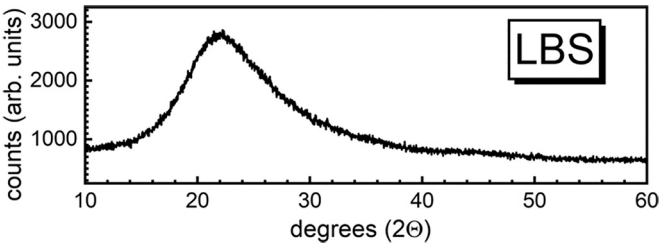

Fig. 2. XRD of the opaque, phase separated, annealed LBS.

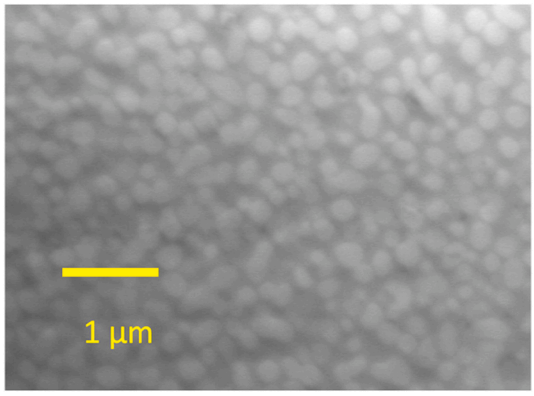

Fig. 3. SEM image of phase separated, annealed LBS glass. Secondary electron imaging .

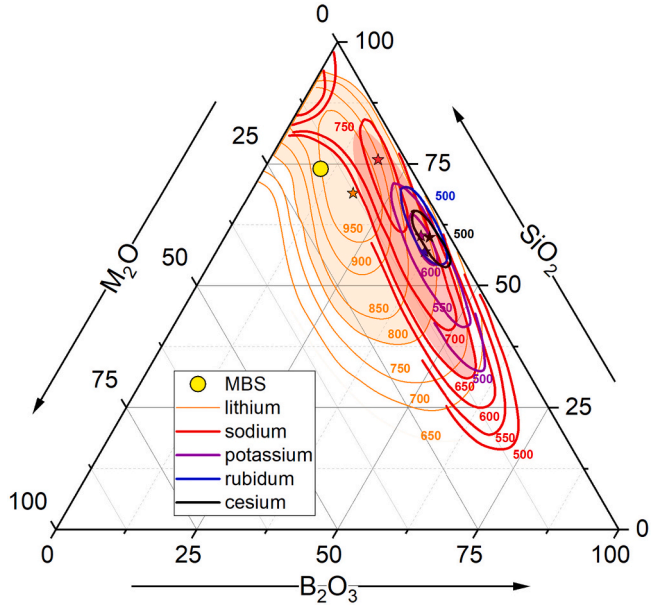

Fig. 4. Ternary diagram showing the range of phase separation for the M_2O-B_2O_3-SiO_2 system at different temperatures. The yellow mark (MBS: $16M_2O$-$10B_2O_3$-$74SiO_2$ glass) is found outside the range of phase separation for M = Na (red), M = K purple), M = Rb (blue), and M = Cs (black), but inside the range of phase separation for M = Li (orange). The plot is based on a figure by Mazurin et al. [7]. The contours reflect the extent of phase separation for different temperatures, stated in °C. (For interpretation of the references to color in this figure legend, the reader is referred to the web version of this article.)

an actual physical interface, is often preceded in alkali borosilicate networks by a more gradual process of clustering and preferential bonding. Earlier studies on low sodium borosilicate glasses showed that variations in the quenching rate, or small compositional changes, could significantly change the connectivity between borate and silicate units [1,6,10,14,53]. As the field strength of the cations decreases further via K to Rb to Cs, the range of phase separation decreases drastically, and is limited to lower and lower temperatures, where the viscosity of the melt is high, and the kinetics will further limit substantial reordering of the borate and silicate units during cooling of the melt. Thus, special consideration will be given to changes in the inter- and intra- connectivity of borate and silicate units, such as a prevalence of B-O-Si or B-O-B and Si-O-Si bonds, when studying the MBS series by NMR, IR, and Raman spectroscopy.

3.2. Glass properties

Table 1 lists selected glass properties, as well as measured structural parameters; density (ρ), glass transition temperature (T_g), refractive index (n_D), fraction of four-fold coordinated boron (N_4), and the vibration frequency of the M^+ cation against its site ($\tilde{\nu}_{M\text{-}O}$). Table 1 also lists parameters that were deduced from experimental values such as molar volume (V_m), packing density (C_g), theoretical and experimental optical basicity (Λ_{th} and Λ_n) as well as the force constant of the M cation – site interactions ($F_{M\text{-}O}$).

The increase in density with increasing alkali size can be explained by the heavier mass of the substituted alkali ions, see also Fig. 5a. Even though some of the K, Rb, and Cs glasses had initially been melted in silica crucibles, their densities and refractive indices show no measurable deviation for Pt or SiO_2-crucible melting. We therefore assume that the combination of very short melting times and high melt viscosities did not dissolve significant amounts of the crucible material. The molar volume increases with increasing alkali size, reflecting on the larger ions' expansion of the network Fig. 5b.

Before calculating the packing density, we must discuss likely coordination numbers (CN) for the various alkali cations, as deduced from the literature [54,55]. As expected, the smallest coordination environment was found for the small lithium ion, with CN(Li^+) = 4 to 4.5 in borate and silicate glasses [56–59]. In alumino-silicates CN(Na^+) = 5 to 7.5 [60], where a lower CN is given for the first coordination sphere, with additional oxygen atoms at slightly larger distances [61]. Thus, low coordination numbers of CN(Na) = 5 can often be found in the literature e.g., for borosilicate glasses [62], but higher CN are stated when more distorted environments are considered as well [55,56,59]. CNs of potassium ions are listed at 5 to 10, e.g., giving CN(K) = 5–7 for borates [63], to 9–10 in alumino-silicate glasses [64] and to an average 8 in a titano-silicate glass [65]. The observed CN range reflects once more on variations in K-O distances and difficulties in separating first order and second order coordination spheres in distorted polyhedra. Literature on Rb-coordination numbers is rare and values of CN(Rb) ≈ 5.5 to 7 for borate glasses [66] are surprisingly low when considering the large size of Rb^+. Asymmetries in the bond length distribution might lead to the undercounting of some ligands of the rubidium cation, especially when comparing the coordination number with its smaller neighbor potassium, CN(K) ≈ 8, and larger neighbor cesium with CN(Cs) ≈ 12. For cesium, different Cs-O distances are well described, for example CN(Cs) = 8 + 4 in a multicomponent borosilicate glass [67], but a similarly high coordination number is also found in borate glasses with CN(Cs) = 10.5 to 13 [55,56]. Thus, we assume a higher coordination number of CN (Rb) ≈ 10 than the referenced CN(Rb) ≈ 5.5 to 7.

The atomic packing density C_g is defined as the ratio between the theoretical volume occupied by the constituent ions and the real volume of a glass. For multicomponent oxide glasses, C_g is given by the general equation:

$$C_g = \frac{\rho}{M_w}\frac{4}{3}\pi N \sum f_i\left(a r_A^3 + b r_O^3\right)$$

with ρ glass density, N the Avogadro number, f_i molar fraction of the i^{th} glass oxide component A_aO_b of molar mass M_i, and ionic radii r_A and r_O for atoms A and O, respectively. The values for the cation ionic radii of Shannon [45] are given in Table 1, as well as of density ρ, and molar volume $V_m = M_w/\rho$. Other effective ionic radii used, relying on data from Shannon [45], are $r_O = 1.35$ Å for oxygen and $r_{Si} = 0.26$ Å for silicon. For boron we considered the presence of B in both coordination numbers 4 and 3 as quantified by ^{11}B NMR, using the expression $r_B = N_4\, r_{B(4)} + (1\text{-}N_4)\, r_{B(3)}$ with $r_{B(4)} = 0.11$ Å and $r_{B(3)} = 0.01$ Å [45].

Table 1 lists the ionic radii for the assumed average coordination number based on studies of borosilicate or borate, and silicate glasses. As can be seen in Fig. 5c, the packing density shows a maximum for the KBS glass but decreases for the lighter ions from Na to Li, and for the heavier ions from Rb to Cs. The mixed cation glasses LNBS and RCBS follow the trend of the single cation glasses.

It is not clear why the density of the KBS glass deviates from the trend shown by the rest of the MBS glasses in Fig. 5a. KBS samples were melted at least twice with newly purchased high quality K_2CO_3. A lid was used

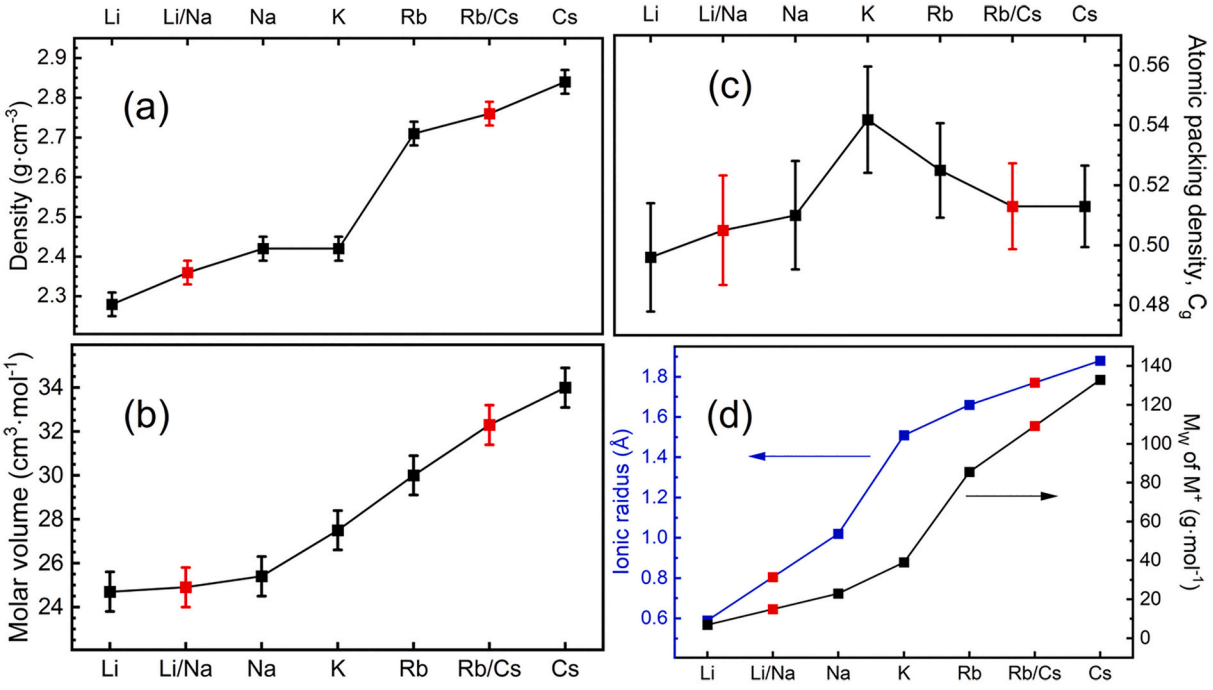

Fig. 5. Plot of (a) density, (b) molar volume and (c) packing density of the MBS glass series; filled symbols correspond to ionic radii for increasing coordination number (CN) as given in Table 1. Red squares represent the mixed glasses. Plotted in (d) are the variations of molar mass of the alkali cations (right axis) and the ionic radius (left axis) as listed in Table 1). Lines are drawn to guide the eye; error margins are smaller than the symbol size. (For interpretation of the references to color in this figure legend, the reader is referred to the web version of this article.)

to reduce evaporation, melting times and temperatures were varied. The density was hardly affected by any of these variations. We note, that Lv et al. also found density values of a KNBS type glass ($56SiO_2$–$14B_2O_3$–$15Na_2O$-$15M_2O$) to be lower than for the corresponding NBS type composition [68]. A nonsystematic change of composition for KBS, like evaporation losses that are only occurring for KBS but not the lighter and heavier MBS glasses seems unlikely. The observed spike in the atomic packing density of KBS likely results from a combination of structural rearrangements of the glass network and the non-monotonic mass increase of the alkali cations. The molar mass increases more steeply for Rb and Cs (Fig. 5d), as d- and f- shells fill up, than the increase of the ionic radii in this series (Fig. 5d). A possible structural origin for the maximum in packing density of the KBS glass will be discussed in more detail in section 3.6 on Raman spectroscopy .

As depicted in Fig. 6, the transition temperature T_g increases with increasing alkali size, which is a contradictory trend to borate [69] or phosphate glasses [70], where a higher field strength of the modifier cation often results in a higher T_g [49]. However, the trend observed here is typical for silicate rich glasses [71]. We note that the T_g of mixed alkali borosilicate glasses of higher modifier content ($M_2O/B_2O_3 = 2.1$), as discussed by Lv et al. [68], shows the same "normal" dependence on the field strength of the modifier cation as known from borate and phosphate glasses, while compositions with lower modifier levels ($M_2O/B_2O_3 = 0.75$) follow the same trend as our study with ($M_2O/B_2O_3 = 1.6$). We note that contrary to density, the KBS glass does not show any abnormal T_g behavior when compared to the other MBS glasses (Fig. 6). Both mixed glasses show a weak mixed alkali effect (MAE) with a slightly lower than expected T_g. The effect is small, but outside the error margins. The MAE is known to be more pronounced when the mixed alkali cations are more distinct in their size and mass, and therefore, the manifestation of the MAE is expected to be small for the Li/Na and Rb/Cs pairs [72].

3.2.1. *Refractive index, polarizability, and optical basicity*

The refractive index increases with increasing alkali size. This is expected, as the refractive index depends on the polarizability of the glass which is a function of the alkali cation polarizabilities α_C; they increase in the order α_{Li}=0.0265 Å^3, α_{Na}=0.178 Å^3, α_K=0.83 Å^3, α_{Rb}=1.427 Å^3, α_{Cs}=2.42 Å^3 [73,74]. In comparison, the network former cations B^{3+} and Si^{4+} are characterized by very low polarizabilities of α_B=0.003 Å^3, α_{Si}=0.033 Å^3. Related to the polarizability is the concept of optical basicity, Λ, as defined by Duffy and Ingram [75,76]. This concept allows quantification of the electron donor power of the glass matrix. The optical basicity relates also to the nephelauxetic effect, the overall oxygen polarizability of the glass, and thus to the refractive index and intrinsic band gap energy. The optical basicity can be calculated from the composition, using an increment system of tabulated oxide basicity data [73,75,77]. The theoretical optical basicity was calculated using the expression:

$$\Lambda_{th} = \sum \Lambda_i x_i \tag{1}$$

where Λ_i is the optical basicity of the constituent oxides, with $\Lambda(SiO_2) = 0.48$, $\Lambda(B_2O_3) = 0.4$, $\Lambda(Li_2O) = 0.84$, $\Lambda(Na_2O) = 1.11$, $\Lambda(K_2O) = 1.32$, $\Lambda(Rb_2O) = 1.41$, and $\Lambda(Cs_2O) = 1.52$ [73,74,78], and x_i represents the proportion of oxygen atoms contributed by each oxide relative to the total number of oxygen atoms in the glass [73].

Theoretical basicity values are listed in Table 1, as are the experimental values that were determined from refractive index and density data using the following Eqs. (2) to (4), based on an empirical correlation between the optical basicity and the oxygen polarizability of glasses [79]:

$$\Lambda_n = 0.7\,\alpha_O - 0.547 \tag{2}$$

To briefly summarize the basic equations, the molar polarizability α_m of a glass can be determined from measured refractive index and molar volume data using the Lorentz-Lorenz equation:

$$\alpha_m = \frac{3V_m}{4\pi N}\cdot\left(\frac{n^2-1}{n^2+2}\right) \tag{3}$$

with *N:* Avogadro number, V_m: molar volume, and *n*: refractive index at infinity. Most often n_D (refractive index at 589.3 nm) is used as an approximation (n_D values are listed in Table 1 for MBS glasses). The electronic polarizability of oxygen ions α_O can be calculated by subtracting the sum of the cation polarizabilities $\sum_i N_C\alpha_C$ from the molar polarizability α_m, and then dividing by the number of oxygen ions , N_O:

$$\alpha_O = \frac{\alpha_m - \sum_i N_C\alpha_C}{N_O} \tag{4}$$

Here, N_C is number of respective cations with cation polarizabilities α_C, as taken from the literature and listed at the start of this section [73,74]. The experimental optical basicity values Λ_n, as derived from the combination of Eqs. (2) and (4), are listed in Table 1 next to the theoretical basicity values Λ_{th}.

As seen in Table 1 and Fig. 7, experimental basicity values are slightly lower than the theoretical data for low basicity glasses; however, for samples containing the heavier alkali analogues the experimental values exceed the theoretical basicity values. It is not clear if using constant cation polarizabilities might be the problem, but overall more and better basicity data are available for the lighter alkali oxides than for the lesser used heavier alkali oxides [73]. As discussed by Komatsu et al. [78], basicity values might have to be adapted for many glass oxides, especially when the original data was obtained from refractivity data of crystalline compounds. The RCBS glass shows a surprising low refractive index compared to the other compositions. The same low n value is obtained for large melt quantities with long-, or small melt quantities with very short-melting times. The density of the mixed glass is slightly lower than interpolation between the values of the RBS and CBS samples would suggest, which might indicate a lower electron density for the mixed glass. Calculating the optical basicity from the oxygen polarizability does not show the RCBS glass as an outlier, but on the trend line of all MBS glasses, especially the RBS and CBS basicity values, indicating that the lower refractive index value might indeed reflect variations in the packing density. Moreover, in the next section it will be shown that nickel speciation of RCBS fits well between RBS and CBS, while later on, NMR and Raman measurements also show good continuity in the structural progression of the heavy alkali glasses.

The optical basicity can also be determined using a probe ion such as Pb^{2+} or Mn^{2+}, which both possess electronic transitions that are very sensitive to the Nephelauxetic effect [25,75,76,79,80]. However, these

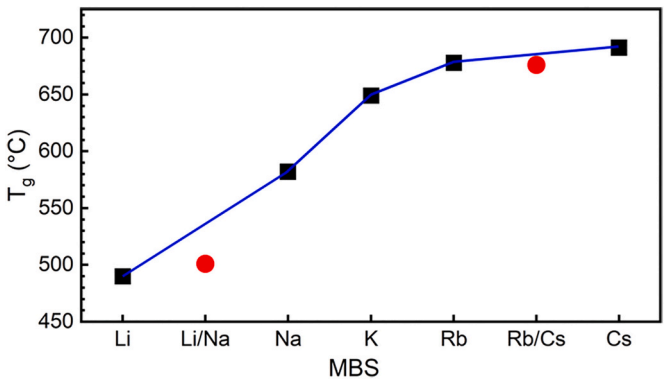

Fig. 6. The glass transition temperature, T_g, of MBS glasses increases with the size of the alkali ion from Li to Cs; the values of the two mixed cation glasses (red circles) show a slight T_g depression due to the mixed alkali effect. Errors are smaller than the symbol size. (For interpretation of the references to color in this figure legend, the reader is referred to the web version of this article.)

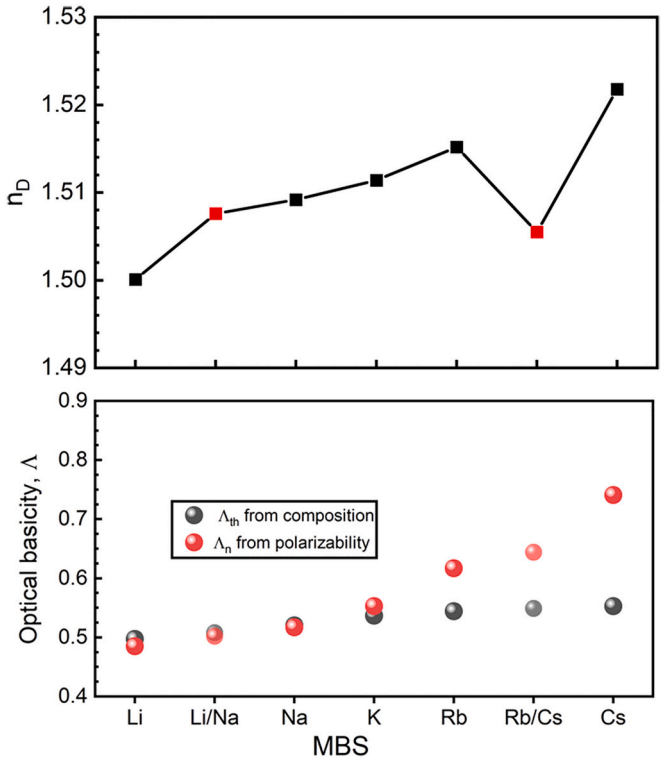

Fig. 7. Alkali dependence of optical properties in 16 M_2O – 10 B_2O_3–74 B_2O_3 MBS glasses. Error bars are smaller than the samples size.

ions might be bonded preferentially to borate over silicate ligands or highly charged sites with more nbOs and thus, show a higher-than-average optical basicity. While Co^{2+} and Ni^{2+} cannot be used to measure the Nephelauxetic effect directly or to quantify the optical basicity, the coordination change from octahedral in low basicity glasses to tetrahedral in high basicity glasses is well known and all MBS samples follow this exact pattern.

3.3. UV-VIS spectroscopy

Changes in silicate and borate speciation with increasing modifier size and basicity correlate with a change in the color and optical spectra of the nickel-doped glasses (see Fig. 8 and Fig. 9).

For glasses, only divalent nickel ions in various distinct coordination sites are discussed in the literature [39,40]. Symmetric octahedral Ni^{2+}

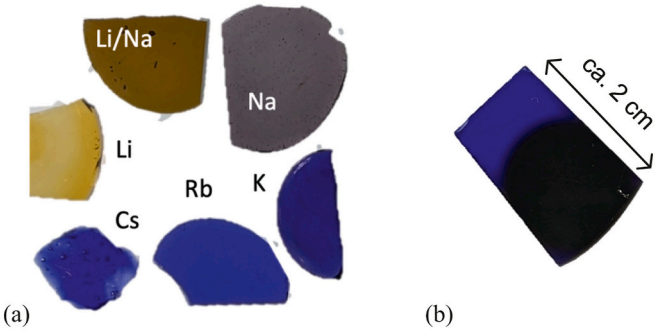

Fig. 8. (a) Photograph of nickel-doped MBS samples, from yellow LBS on the left, clockwise to blue CBS. The samples are about 1 cm wide and on average 3–4 mm thick, with 2 mm for the quenched LBS, and (b) Ni-doped CBS sample after XRF analysis. The X-ray induced darkening is clearly visible at the right side of the sample. (For interpretation of the references to color in this figure legend, the reader is referred to the web version of this article.)

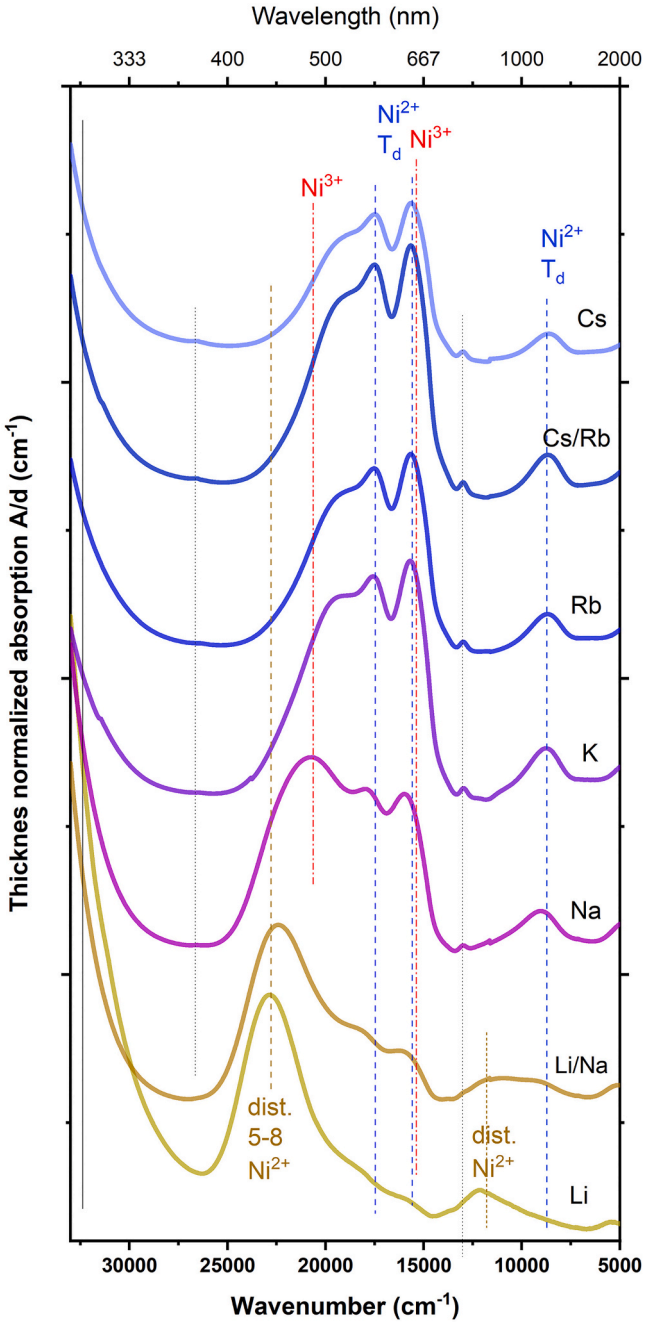

Fig. 9. Optical spectra of alkali borosilicate glasses doped with 0.1 mol% Ni_2O_3. Selected frequencies are identified by vertical lines for use as reference points. Spectra are normalized to the thickness of the sample (=optical density). Peaks marked by "dist." correspond to distorted Ni^{2+} sites, while T_d indicates regular tetrahedral sites. The LBS spectrum was taken from a transparent quenched area.

typically results in light green colored glasses and crystals [81,82], while tetrahedral Ni^{2+} has been identified as source for the intense brown to purple colors in glasses of higher optical basicity [38,39]. A third transitional yellow to orange coordination of either a very distorted octahedral [81], eight-fold pseudo-tetrahedral [30,32,83] or fivefold coordination [40] is also discussed in the literature.

Interestingly, Bamford excluded the possibility of trivalent nickel ions due to high ionization energies, and we are not aware of any studies challenging this view, despite the fact, that Co^{3+} has been successfully prepared first by Dietzel and Coenen and then later by Möncke and Ehrt [42,43,84]. Möncke and Ehrt also found that glasses of higher optical

basicity in which nickel ions were more likely tetrahedrally than octahedrally coordinated, could be photo-oxidized to $(Ni^{2+})^{+}$ by UV and X-ray irradiation, while nickel ions in low basicity glasses were photo-reduced to $(Ni^{2+})^{-}$ [43].

Photographs in Fig. 8 show changes in the color of the samples from yellow (LBS) to brown (LNBS), to purple (NBS), to blue (KBS to CBS). No changes in the color were apparent between annealed and quenched glasses. The UV–Vis spectra in Fig. 9 seem to show a continuous transformation from yellow LBS with a band maximum at 440 nm (22,800 cm^{-1}) to a more complex spectrum with a pronounced double peak at 575 nm (17,400 cm^{-1}) and 640 nm (15,600 cm^{-1}) and a high energy shoulder for the blue high basicity glasses. The electronic spectrum of yellow LBS is in agreement with a distorted transitional coordination with four close ligands and several ligands at a greater distance, such as described for the eight-fold pseudo-tetrahedral, T_8 [30,32,83], five-fold [40] or distorted octahedrally [81] coordinated divalent nickel ions. Symmetric octahedral nickel would give a green glass, as in annealed low sodium borosilicate glass $74SiO_2$–$4.3Na_2O$-$20.7B_2O_3$-$1Al_2O_3$ of low optical basicity [82]. The band intensity for the octahedral Ni^{2+} ion would also be lower, since the Laporte selection rule is stronger enforced for centrosymmetric than for distorted symmetries [76]. The band maximum would be around 400 nm (25,000 cm^{-1}), and not the observed 440 nm, while the low energy bands would have higher energies, e.g., around 715 nm (14,000 cm^{-1}) and 1250 nm (8000 cm^{-1}), instead of the observed 835 nm (12,000 cm^{-1}) and 1590 nm (6300 cm^{-1}). For LBS, we assume that this distorted, high coordination divalent nickel species is the main absorbing species.

The mixed Li/Na sample shows spectral features of the LBS and NBS glasses, noting the emergence of bands at 630 nm (15,900 cm^{-1}) and 560 nm (17,800 cm^{-1}). The main band appears to shift from 440 nm in LBS to 450 nm (22,300 cm^{-1}) in LNBS, to 480 nm (20,800 cm^{-1}) in NBS. The glasses appear brown to deep purple. As the bands of higher coordinated Ni^{2+} decrease in intensity in favor of tetrahedral Ni^{2+}, the glasses turn blue, as is also known from crystalline materials [40,81]. The main band is split in two maxima peaking at 575 nm (17,400 cm^{-1}) and 640 nm (15,600 cm^{-1}). It should be noted that tetrahedral nickel in crystals does not show the strong shoulder at higher energies centered around 480 nm (20,800 cm^{-1}) in the MBS glasses.

The glass literature does not discuss any other oxidation states of nickel than Ni^{2+}. However, it is known that a high basicity glass matrix supports higher oxidation states of polyvalent dopants. Furthermore, nickel doped NBS glass shows photo-oxidation of Ni^{2+} to $(Ni^{2+})^{+}$ when exposed to UV or X-ray irradiation [43]. The induced spectra show negative, or no absorbance change around 440 nm (23,000 cm^{-1}) and 900 nm (11,000 cm^{-1}) which coincides with the absorption band of distorted, high coordination Ni^{2+} as found in LBS. Strong bands of $(Ni^{2+})^{+}$ appear at 480 nm (21,000 cm^{-1}) and 670 nm (15,000 cm^{-1}).

Fig. 10 shows the induced absorption spectra, that is, the spectrum taken before irradiation is subtracted from the spectrum after 100 h UV light irradiation by an XeHg-lamp. The two spectra are of a soda lime silicate glass NCS ($74SiO_2$-$10CaO$-$16Na_2O$) and a sodium borosilicate glass of the same composition as sample NBS of the current study. As discussed in references [43, 44], the negative induced absorption corresponds to electronic transitions of higher coordinated Ni^{2+}, whose concentration decreases under irradiation as this species is photo-oxidized to $(Ni^{2+})^{+}$. While the induced absorption is slightly less intense in NBS, the comparison with NCS shows fundamentally the same processes for both glasses.

Literature on trivalent and tetravalent nickel species is rare, but the few reported spectra of higher oxidized nickel species confirm the spectral overlap of their electronic transitions with those of various divalent nickel species. Sanz-Ortiz et al. [85] describe Ni^{3+} in a distorted octahedral environment in $LaAlO_3$ crystals with absorption bands at 10000 cm^{-1} (1000 nm), a broad band around 25,000 cm^{-1} (400 m) and another narrower band at 40000 cm^{-1} (250 nm). D'Amario et al. [86,87] studied higher valent nickel species in NiO nanoparticles and

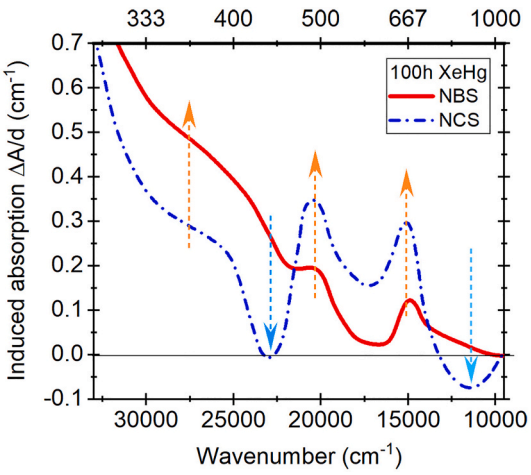

Fig. 10. Induced optical spectra of a nickel doped NBS glass (solid red line, 0.3 mol NiO) after XeHg-lamp irradiation, derived by subtracting the spectrum taken before irradiation from the spectrum taken after irradiation. The induced spectrum of NCS ($74SiO_2$-$10CaO$-$16Na_2O$ with 0.3 NiO in mol%, broken blue line), is included for comparison, as the photo-oxidation of Ni^{2+} to $(Ni^{2+})^{+}$ is notably stronger, and even the negative induced absorption of Ni^{2+} bands is evident. Data from Ref. [43, 44]. (For interpretation of the references to color in this figure legend, the reader is referred to the web version of this article.)

assign broad absorption bands centered around 400–500 nm (25000–20,000 cm^{-1}), 730 nm (13,700 cm^{-1}) and 900 nm (11,100 cm^{-1}) to Ni^{3+}, but also bands due to Ni^{4+}, which include split bands around 400 nm (25,000 cm^{-1}) and broad bands near 680 nm (14,700 cm^{-1}) and 840 nm (11,900 cm^{-1}). Vasileva et al. [88] assigned electronic transitions to octahedral and tetrahedral nickel in the divalent and trivalent states in crystals. Davidson et al. [89] compare Ni^{2+} and Ni^{3+} in NiO and related compounds by UV–Vis, XPS and EPR spectroscopies.

Fig. 11a shows the overlapping UV–Vis spectra of MBS glasses normalized to the sample thickness, and Fig. 11b depicts a similar plot normalized to the maximal band intensity. Interestingly, the intensity of the 500 to 670 nm band envelope is highest for KBS and decreases with increasing optical basicity via the Rb- to the Cs-glass. Since the relaxation of the selection rules for tetrahedral coordination increases the extinction coefficient substantially [76,90], the reduced intensity might reflect on fewer tetrahedral Ni^{2+} in favor of more octahedral Ni^{3+} in the high basicity glasses RBS and CBS. It should be noted that the background scattering in LBS results in an artificial high apparent intensity for Fig. 11a. The d-d transition of Ni^{2+} in LBS is lowest, as expected for the transitional coordination [31–33,83].

Band deconvolution was not attempted as we feel that we need more information on the many simultaneously present nickel species, each of which would be fitted with several overlapping Gaussian bands. Multi component analysis, as applied before successfully by Gitter et al. [30], suggests the presence of at least three different species in the MBS series. Electron paramagnetic resonance (EPR) spectroscopic measurements on MBS samples were non-conclusive and are not shown here; EPR is very sensitive to typical impurities such as Fe^{3+} or Mn^{2+}, and their signals are superimposed on any weak Ni^{3+} contributions. EPR showed that these impurities are present in very low concentrations only, even forbidden transitions of the d^5-ions characteristic sextet signal centered near $g \approx 2.1$ are observable [25]. However, the broad sextet overlaps with any Ni^{3+} signals that are also expected around g-values of 2.04 to 2.25.

3.4. NMR

^{11}B NMR provides a powerful tool for the identification of borate species in boron containing glasses and crystals [1,20,21,24,91].

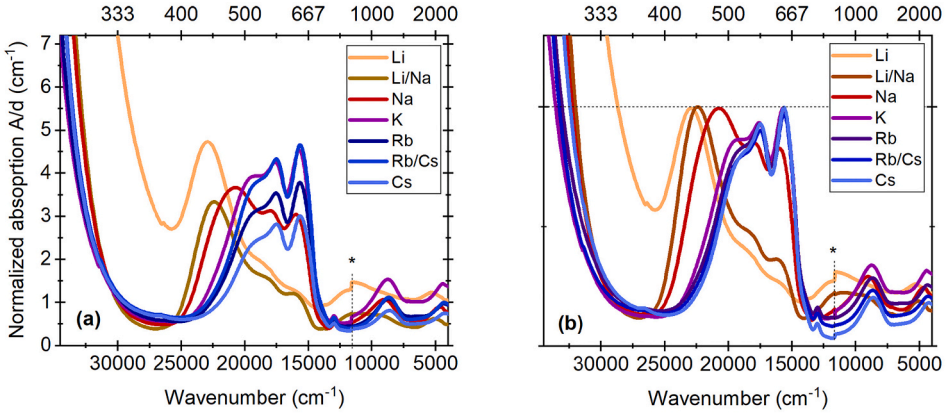

Fig. 11. Absorption spectra of Fig. 9, normalized in (a) to the sample thickness, but plotted without stacking, and in (b) normalized to the maximal peak height (450 nm for Li and Na samples and to 670 nm for K to Cs glasses). The asterisk is an artifact of instrumentation.

Nowadays, the high magnetic fields available in modern instruments allow full separation of the resonances associated with triangular and tetrahedral borate species [24]. Here, the peaks due to trigonal boron (B_3) span from roughly 5 to 20 ppm while those of tetrahedral boron (B_4) span roughly from −5 to 5 ppm (Fig. 12) [24,53]. Careful fitting of the signal in these regions provides quantification of B_3 and B_4 units, while the resulting peak positions for B_4 resonances are also very sensitive to mixing between borate and silicate groups. Within the trigonal boron signal region, more than one B_3 resonance is commonly found. For example, B_3 units in non-ring environments, that is the trigonal boron found outside of geometrically constrained borate superstructural units, is found at lower MAS NMR shifts [24,53]. This is the case for these glasses, and as a result of careful fitting of MAS NMR lineshapes, as well as evaluation of ^{11}B triple-quantum MAS (3QMAS) NMR, ring and non-ring B_3 groups are identified (see SI Figs. 1 and 2.). In the Li containing glass, the non-ring signal around 10 ppm is only a shoulder on the B_3 resonance, and the majority of the B_3 signal is due to ring-type BO_3 groups. A high fraction of ring B_3 units (27% ± 5), in conjunction with a significantly more positive shift of the B_4 resonance for quenched LBS may be indicative of phase separation or at least a significant manifestation of preferential bonding of the B-O-B type [92]. The total signal for trigonal boron falls away swiftly with increasing alkali size, ultimately comprising <10% of the total B speciation, further complicating analysis of the trigonal boron lineshapes in ^{11}B MAS NMR (SI Fig. 3). Although the fitting of these two weaker signals in these data is not unique, this provides some support for our assertion that limited nbO in these glasses is predominantly located on silicate groups.

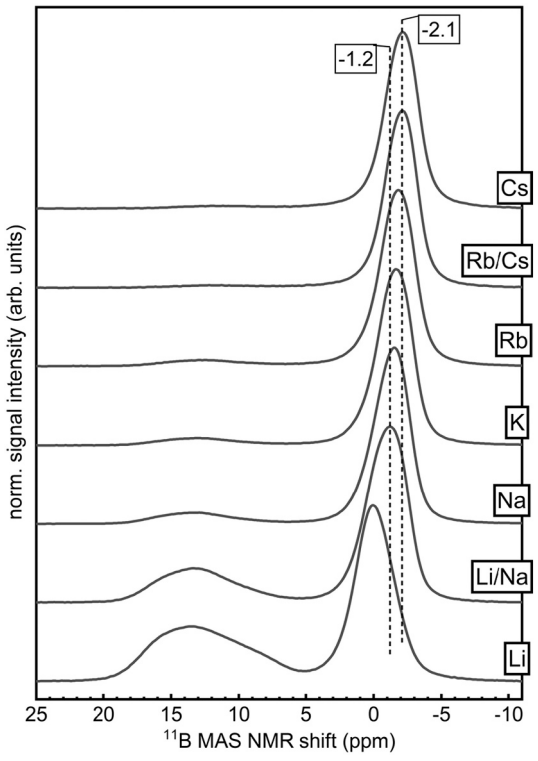

Fig. 12. ^{11}B MAS NMR spectra for annealed alkali borosilicates, compared to quenched LBS.

Quantified by signal integration, the fraction of four coordinated boron, N_4, increases sharply from Li to Na then slowly up to Cs (see Table 1). The center of the tetrahedral boron band, which is due to relatively small 2nd-order quadrupolar shifts for BO_4 polyhedra and hence reflects approximate chemical shifts, moves slightly to lower ppm as the size of the alkali ion increases. The resonance for the mineral danburite, where one borate tetrahedron is joined at three corners to silicate tetrahedra, and on the fourth to one more borate tetrahedron B_4, has been reported at −0.7 ± 0.2 ppm [93]. The same authors report the peak for the mineral reedmergnerite, where one tetrahedral borate B_4 is joined to 4 silicate tetrahedra, to be −1.9 ± 0.2 ppm. Therefore, the upfield shift in the B_4 resonance as a function of alkali size (Fig. 12) could be attributed to increased mixing of silicate and borate polyhedra (i.e., Si-O-B bonds). However, in this series where the alkali size variation is extreme, the effect of the field strength of the modifier could also drive this behavior. Correlation studies utilizing 2D NMR would be well suited for investigating the degree of heteropolar bonding as a function of alkali cation. Neutral B_3 units are likely the borate species participating in ring arrangements as seen by NMR.

3.5. *Infrared spectroscopy*

The spectrum of quenched LBS in Fig. 13 closely resembles that of pure Pyrex® [2]. The strongest feature in the infrared absorption spectrum of pure SiO_2 is at 1100 cm^{-1} with a shoulder around 1200 cm^{-1} belonging to the asymmetric stretching of Si-O-Si bridges connecting fully polymerized silicate tetrahedra [94]. The bending of these Si-O-Si linkages is seen at 806 cm^{-1}, while the band with a maximum at 1390 cm^{-1} is attributed to the asymmetric stretch of neutral trigonal borate units, $B\emptyset_3^0$ [15].

The shoulder between 955 cm^{-1} (LBS) and 915 cm^{-1} (RBS) suggests the presence of tetrahedral borate species – as seen by NMR spectroscopy, overlapping with signals due to silicate tetrahedra with both one (Q^3) and two (Q^2) non-bridging oxygen atoms [2]. Note that Q^n denotes silicate tetrahedra with n bridging oxygen atoms bonded to any glass former, Si or B. These features indicate that the high field strength Li^+

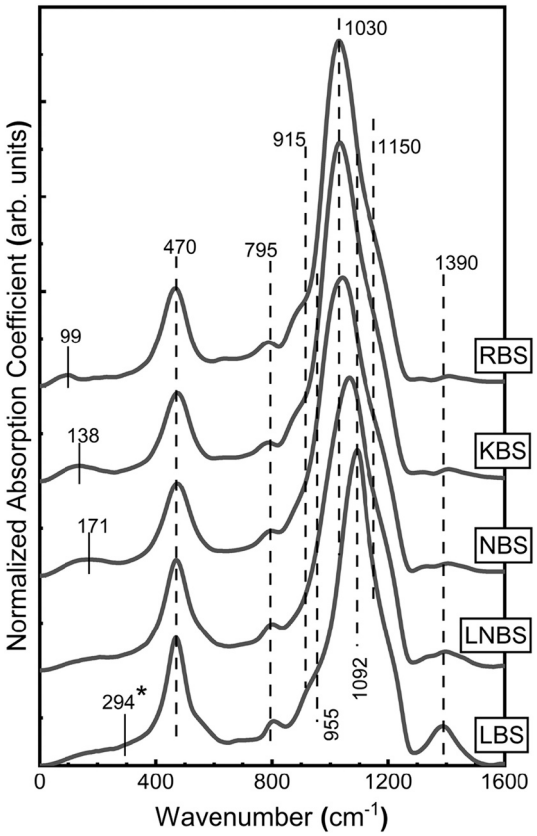

Fig. 13. Infrared absorption coefficient spectra obtained for annealed alkali borosilicates, compared to quenched LBS. The asterisk at 294 cm^{-1} marks the value for the Li^+ motion band obtained by extrapolation of a linear fit applied to the frequency of the Na^+, K^+, and Rb^+ cation motion bands (see Fig. 14).

ions favor the bonding to non-bridging oxygen on silicate tetrahedra since a significant portion of the boron units remain unmodified as $B\emptyset_3^0$ (peak at 1390 cm^{-1}). The high number of Q^2 groups might also be enforced by the higher fictive temperature of the quenched glasses, for which the metaborate equilibrium is on the side of the lower trigonal rather than tetrahedral borate units [11,53,95–98]. In conjunction with the transfer of nbO's to silicate units, the disproportionation equilibrium $2\ Q^3 \rightleftharpoons Q^2 + Q^4$ - also shifts to the right with increased fictive temperature [99,100]. Increasing alkali ion size leads to a downshift of the Si-O-Si asymmetric stretching envelope from 1092 cm^{-1} for Li to 1030 cm^{-1} for Rb. At the same time, the $B\emptyset_3^0$ signature at 1390 cm^{-1} gradually loses intensity and almost disappears for M = Rb, as it is replaced by a shoulder at around 915 cm^{-1} associated with the asymmetric stretch of $[B\emptyset_4]^-$ units [15]. The 850–1250 cm^{-1} envelope does not change significantly between the K and Rb spectra, noting that the small size of the CBS samples did not allow for reliable infrared reflectance measurements for CBS.

We conclude from the infrared spectra that for alkali ions larger than Na, nearly all the boron atoms are modified by the alkali oxides to form $[B\emptyset_4]^-$ borate tetrahedra, in agreement with the ^{11}B NMR results. Theoretical considerations subsequently dictate that approximately 1 in 6 silicate tetrahedra are modified to likely Q^3 units with one non-bridging oxygen atom, assuming no further disproportionation. Beside the tetrahedral borate shoulder at ~915 cm^{-1} and the expected contribution of the fully polymerized silicate tetrahedra in the high frequency shoulder at ca. 1200 cm^{-1}, the main 1030 cm^{-1} band for KBS and RBS is relatively symmetric; this suggests for these heavier alkali ions that any modified silicate tetrahedra are probably of the Q^3 type. Contributions of the Si-O-B_4 type are expected to overlap with the stretching modes at 930 cm^{-1} and for Si-O-B_3 at 1150 cm^{-1}, and the bending modes of Si-O-B bridges show at 670 cm^{-1} [14,92,101].

Far-infrared studies of oxide glass forming systems reveal information on the environment of metal cation modifiers [56,102,103]. The frequency of the FIR band has been shown to be proportional to the inverse square root of the mass of the modifier cation. The far-infrared band measured for the glasses with larger cations was well separated, allowing the maximum value to be determined with certainty, while the Li^+ motion band overlaps with network deformation modes (Fig. 13).

By applying a linear fit to the values obtained for Na, K, and Rb and extrapolating to lower mass values, the position of the Li motion band is approximated to be around ~294 cm^{-1} as indicated in Fig. 13. The fit was extrapolated also to higher mass values to obtain a value for the Cs glass, since the size of the CBS sample did not allow for reliable infrared reflectance measurements and, in any case, the instrument used in this study does not allow measurements in the region of Cs-O stretching. The M-O frequency values obtained by extrapolation are indicated by open squares in Fig. 14, and in the respective figures discussing structure property correlations in section 3.7.

3.6. Raman spectroscopy

The Raman spectra of MBS glasses are depicted in Fig. 15, where the high frequency range agrees well with the structural picture depicted by infrared spectroscopy. The signature of trigonal boron groups is apparent in quenched LBS as a broad and weak feature at ~1450 cm^{-1} which decreases in intensity for the heavier analogue NBS, until it fully disappears for KBS and beyond. In LBS, the presence of Q^2 silicate species is suggested by the ~945 cm^{-1} feature, which appears to be absent from the M = Na to Cs glass spectra. The broad asymmetric high frequency band in the Li glass with a maximum at 1054 cm^{-1} can be considered as the convolution of the Si-O stretching in Q^3 silicate units (with one nbO = O^-) and the asymmetric stretching of Si-O-Si bridges connecting fully polymerized Q^4 units [104]. As discussed before for the infrared spectra, Si-O-B bridges might cause additional signatures at higher (Si-O-B_3) or lower (Si-O-B_4) frequencies, depending on the bond strength of trigonal or tetrahedral borate units respectively [2,3,14,26,92,101].

The activity around ~945 cm^{-1} for M = Li is replaced by a subtle feature at ~905 cm^{-1} for M = Na-Cs. This feature trends with the 955 cm^{-1} shoulder in the infrared spectra and is attributed to the Raman activity of the asymmetric stretch of borate tetrahedra (B_4). The maximum of the high frequency envelope becomes well defined at ~1080 cm^{-1}, and this is assigned to the Si-O stretching in Q^3 silicate units, this mode being strongly polarized (Fig. 16). Considering the glass composition $16M_2O–10B_2O_3–74SiO_2$, it is noted that most silicate tetrahedra are expected to be unmodified (Q^4); this is because M_2O is primarily reacting with $2B\emptyset_3$ to form $2\{[B\emptyset_4]^- \cdots M^+\}$ units and only the remaining 6–7 mol M_2O will be available to form nbO's on silicate tetrahedra, assuming no nbO on trigonal boron [10]. The Raman cross

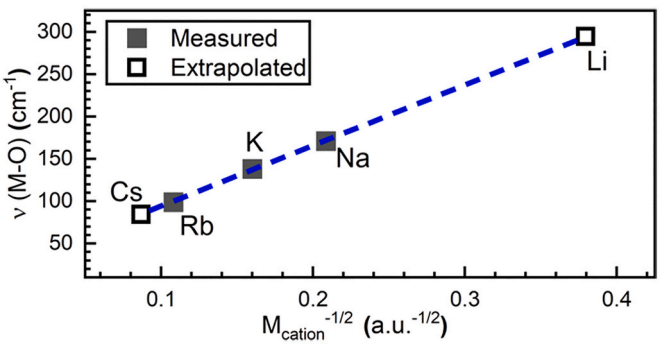

Fig. 14. Plot of the frequency of the far-infrared band versus the inverse square root of the alkali cation mass. The values of the Li and Cs motion bands were determined by extrapolation from the clearly linear relation for Na, K, and Rb.

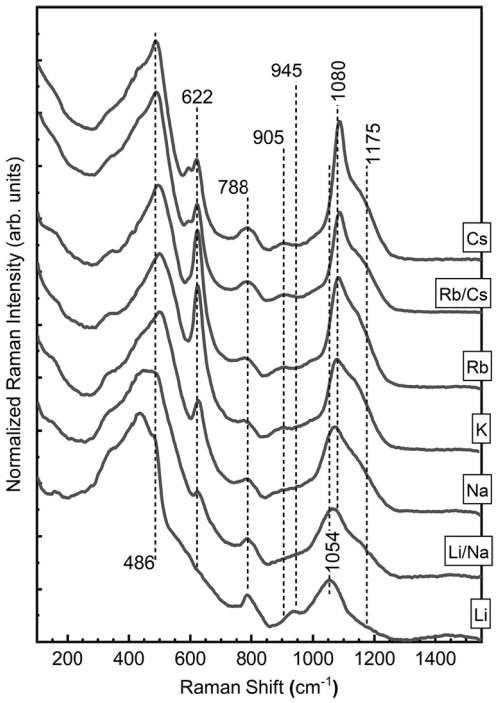

Fig. 15. Raman spectra of annealed alkali borosilicate glasses MBS, compared to quenched LBS, area normalized over the interval 100–1550 cm^{-1}.

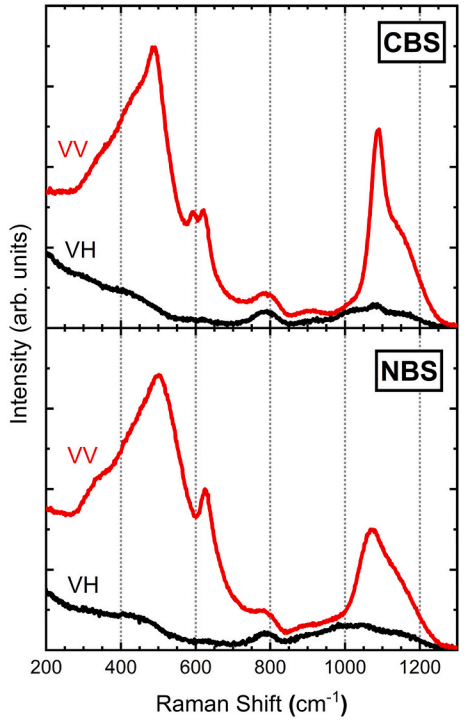

Fig. 16. Polarized Raman spectra for Cs and Na borosilicate glasses. The parallel polarized spectra are denoted by VV and presented in red, while the perpendicular polarized spectra are denoted VH and presented in black. (For interpretation of the references to color in this figure legend, the reader is referred to the web version of this article.)

section is much greater for SiO_4-tetrahedra with nbO's than without (Q^4), and thus, despite a smaller population compared to their fully polymerized counterpart, scattering from Q^3 species is of high intensity [2]. The asymmetry of the high frequency shoulder is likely due to a combination of contributions from Q^4 species connected to borate polyhedra, roughly between 1130 and 1150 cm^{-1}, and Q^4 species connected to four other silicate entities, roughly between 1160 and 1190 cm^{-1} [11].

Spectral activity in the 750–850 cm^{-1} Raman range, while typically associated with the bending of Si-O-Si linkages within all glasses [1–3,94], may have additional borate contributions in glasses with high field strength modifier alkali cations. NMR results for the quenched Li glass quantifies the fraction of boron atoms in rings at circa 27% (±5%). A review by Wright [105] of vitreous and crystalline borates reports that no ring B_3 units with nbO's are found whenever a ring $BØ_3$ could transform into to a ring $[BØ_4]^-$ unit. These trigonal boron in rings may exist in boroxol rings or similar borate rings containing 1 or 2 borate tetrahedra which have characteristic ring breathing modes at 805 cm^{-1} as well as 780–770 cm^{-1} and 760–750 cm^{-1}, respectively [106,107].

For quenched LBS, the sharp asymmetric feature at 780 cm^{-1} indicates the presence of borate rings with one $[BØ_4]^-$ unit and the prominent feature at ~430 cm^{-1} arises from the vibrational activity of 5 and 6 membered silicate rings as observed in pure SiO_2 [2]. In a similar fashion, a distinct shoulder at 486 cm^{-1} in LBS can be attributed to 4-membered silicate rings (D_1) [2,3]. The region between 500 and 700 cm^{-1} can be viewed as consisting of heavily overlapping contributions from covalently linked network former polyhedra involved in bending and stretching motions [2,3,101,108]. As Na is substituting for Li, a new feature develops around ~622 cm^{-1} and becomes well defined in the NBS spectrum. This has been previously discussed as belonging to the ring breathing mode of danburite type rings consisting of two adjacent borate tetrahedra and two silicate tetrahedra [1,4,5,11].

Exciting here, is the development of an additional feature at 593 cm^{-1} that becomes differentiable in the CBS glass (Fig. 17). This feature

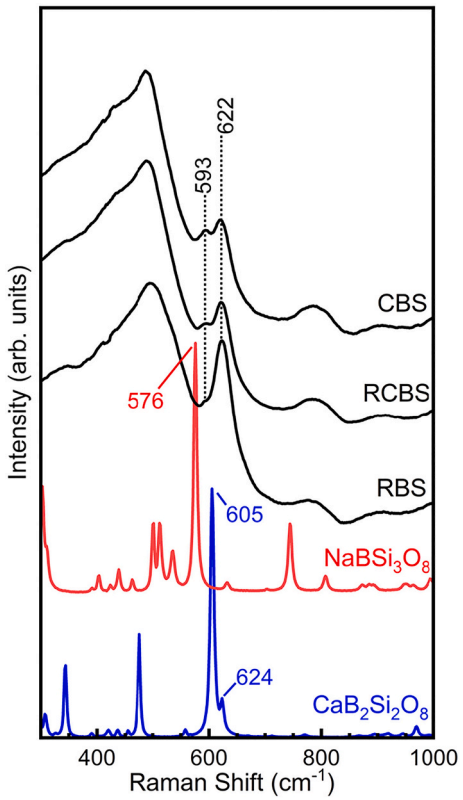

Fig. 17. Raman spectra of Rb, Cs, and mixed Rb-Cs borosilicate glasses compared to Raman spectra of danburite ($CaB_2Si_2O_8$) and reedmergnerite ($NaBSi_3O_8$) reference materials plotted over the interval 300–1000 cm^{-1} to highlight the region where ring breathing modes are active.

is first seen as a slight kink in RBS and might even be present in the KBS spectrum, though hidden by overlapping bands. This feature is both sharp and polarized (Fig. 16), like the danburite ring breathing mode, and several explanations can be discussed for its origin. First, the metaborate ring anion persists in binary borate glasses and crystals with large alkalis [109,110]. This ring consists of three trigonal boron atoms linked together where the non-ring oxygen atoms are non-bridging, and has a characteristic ring breathing frequency around 605 cm^{-1}. Since NMR confirms that nearly all boron atoms are tetrahedrally coordinated and in the absence of the asymmetric stretch of trigonal boron at high frequencies of the vibrational spectra, we can rule out this assignment. Furthermore, although the ^{11}B MAS NMR signal for trigonal boron is very weak in most of these glasses (Fig. 12), there does not appear to be any conclusive evidence for nbO on B_3 groups, in agreement with earlier studies [10].

Another explanation could be in terms of silicate rings consisting of three silicate tetrahedra that exist in pure SiO_2 [23]. Considering that the ring breathing mode of this structure displays Raman activity at ~605 cm^{-1} for SiO_2 glass, and gives a distinct feature at 595 cm^{-1} for Cs_2O-5SiO_2 glass [104], the presence of 3-membered silicate rings could thus also characterize MBS glasses with M = Rb, Cs. This silica ring is known from pure silica, as well as for low alkali borosilicate glasses that consist only of Q^4 units [92], but is absent in NBS. Incidentally, a very weak spectral feature in the quenched LBS glass is evident in Fig. 15 at 607 cm^{-1} and this might be attributed to such 3-membered silica rings in the silica rich, Li-poor subnetwork. As seen in Fig. 17, the new band at 593 cm^{-1} gains relative intensity at the expense of the feature at 622 cm^{-1} from M = Rb to M = Cs. As noted above, the 622 cm^{-1} feature results from the ring breathing mode of the borosilicate ring known to exist in the mineral danburite, as well as in NBS glass [2,5,19]. A second mineral containing borosilicate rings is reedmergnerite, where the borosilicate ring consists of three silicate tetrahedra and one borate tetrahedron. Measured reference materials in this study give the ring breathing mode of reedmergnerite at 576 cm^{-1} and that of danburite at 605 cm^{-1} (Fig. 17). It should be noted that the danburite mineral shows 2 Raman ring breathing modes at 602 cm^{-1} and 625 cm^{-1}, the first for the more symmetric ring with alternating Si and B based tetrahedra, and the smaller one at higher frequencies for the distorted ring with 2 adjacent boron and 2 adjacent Si based tetrahedra [5,18]. This results in an energy separation of approximately 31 cm^{-1} between the breathing modes of reedmergnerite and danburite ring structures. Such separation in energy for these borosilicate rings is in very good agreement with reports by Manara et al. [5] who finds the corresponding frequencies of 586 cm^1 (reedmergnerite) and 614 cm^{-1} (danburite), yielding a difference of 28 cm^{-1}. A similar frequency separation of 29 cm^{-1} is observed for the bands in this range for the large alkali variations of MBS, thus offering another assignment for the new Raman feature.

While the 593 cm^{-1} peak for M = Rb to Cs is fully consistent with the formation of 3-membered silicate rings, one cannot rule out some contribution from reedmergnerite type rings in alkali borosilicate glasses with large alkalis (Rb, Cs). Such a trend could be due to a packing problem encountered for large alkalis associated with danburite type rings. The present spectra imply that with increasing alkali modifier size beyond potassium, the occurrence of danburite rings containing adjacent charged borate tetrahedra decreases. This may be driven by charge repulsion between the two alkali metal ions needed to charge balance the connected borate tetrahedra. Through the lens of the modified random network model, the larger alkali cations in the same channel may seek a far enough separation distance that results in environments unfavorable to the formation of borosilicate rings containing adjacent $[B\emptyset_4]^-$ units but favorable to rings containing only one $[B\emptyset_4]^-$ [111], or to non-ring $[B\emptyset_4]^-$ units coexisting with pure 3-membered silicate rings.

3.7. Structure property correlation

As expected, the structure of the quenched, though not yet visibly phase separated LBS glass was found to deviate from the other MBS samples that looked clear and homogenous even when annealed. According to ^{11}B NMR, the borate network of LBS consists to 43% of neutral trigonal $B\emptyset_3$ units which means that LBS has roughly a third less charged $[B\emptyset_4]^-$ tetrahedra than the heavier analogues of the MBS series. Since NMR does not indicate the presence of asymmetric B_3 groups with nbOs, these spectroscopic findings require that the remaining modifier ions are in turn interacting with the silicate network. Here, we argue that the Li^+ ion having a high field strength favors a high concentration of negative charged sites, such as non-bridging oxygen atoms. This preference triggers the following disproportionation reaction in the silicate network with the Li^+ ion favoring the right-hand side of the equation:

$$2Q^3 \rightleftharpoons Q^2 + Q^4 \quad (5)$$

Both NMR and vibrational spectroscopy for LBS show more homonuclear B-O-B and Si-O-Si bonds, in agreement with a high degree of preferential bonding in the quenched samples, turning into visible phase separation in slowly cooled LBS samples [92]. In analogy to NBS glasses and the description of Sastry and Hummels [51], and in agreement with our spectroscopic findings, we assume that quenched LBS glasses show preferential bonding of borates and silicates, with clustering of modified silicate (Q^2, Q^3) and borate units near lithium ions, and lithium poor silica rich areas (Q^4). Annealing leads to visible phase separation in LBS glasses into soluble Li-borate rich droplets, which still contain considerable amounts of modified silicate within a chemically more resistant, silica rich phase. The latter is also reflected by visual and SEM inspection of the LBS sample. The very low T_g of the LBS glass is a manifestation of the weaker borate network compared to the silica sub-network, as often observed for phase separated glasses [53,92], and reflects overall the lower glass connectivity because of the lower number of $[B\emptyset_4]^-$ tetrahedra and more non-bridging oxygen atoms compared to the other glasses.

Glasses in the MBS series, with M = Na to Cs, do not phase separate and their structure is based on a more modified borate network with predominantly charged $[B\emptyset_4]^-$ tetrahedra. With decreasing field strength of the modifier cation, we find a small but significant increase in the concentration of $[B\emptyset_4]^-$ from NBS ($N_4 = 0.88$) to CBS ($N_4 = 0.97$). Contrary to the small Li^+ cation, the lower field strength M^+ cations favor a more homogeneous distribution of negative charge. Equilibrium (5) shifts toward the side of Q^3 groups, even though starting with a significant higher fraction of Q^4 and lower fraction of modified Q^3 compared to LBS.

The glass transition temperature of modified glasses depends on the connectivity of the network polyhedra and the cross-linking ability of the modifier cations [112]. While field strength only offers an approximation based on the cations charge and radius, the force constant is derived from experimental data, i.e., from far infrared cation motion bands. The force constant, $F_{M\text{-}O}$, allows even comparison of divalent alkaline earth and transition metal ions in metaborate glasses, where the simplified concept of field strength falls short [17]. In binary alkali borate and phosphate glasses, with fixed network modifier to network former (NWM:NWF) ratio, the T_g decreases with decreasing field strength of alkali cation [17,70,112]. The reverse trend is however typical for silicate glasses [71], in agreement with the observations of the current study (Fig. 18), although borosilicate glasses with higher modifier and borate content show a higher T_g when the modifier has a higher field strength [68]. The T_g of MBS glasses increases as the field strength of the modifier alkali cation decreases from Li to Cs (see Fig. 18). This suggests that changes in the covalent structure induced by modifier cations have a greater effect on the rigidity of the network than the variation in the ionic cross-linking strength provided by the monovalent cations. NMR and infrared absorption spectra indicate that the increase in T_g may be due to an increasing degree of polymerization, as more B_4 species form at the expense of units with a lower connectivity, such as B_3, Q^3 or even Q^2 species. The fraction of four-fold coordinated

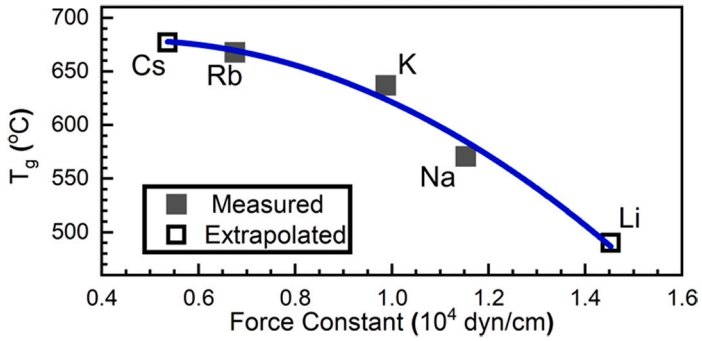

Fig. 18. Correlation between the glass transition temperature, T_g, and the modifier cation-oxygen force constant, $F_{M\text{-}O}$, in MBS glasses. Force constant values calculated for Li and Cs were based on the extrapolated frequency values from Fig. 14. The line is a guide to the eye only.

boron, N_4, as determined by NMR trends well with T_g when these quantities are plotted as a function of the alkali cation field strength (Fig. 19). The logarithmic scale is used to better highlight the small differences in field strength and corresponding properties that occur for the larger modifier cations, compared to the larger differences seen for the smaller ions.

As mentioned before, a weak mixed alkali effect is observed for LNBS and RCBS as a small but significant T_g depression (see Fig. 6), while similar effects are not apparent for density (Fig. 5a), molar volume (Fig. 5b) or packing density (Fig. 5c), where large changes in mass and structural reordering are more prominent. The small T_g depression for the mixed cation glasses is more significant when considering that both mixed glasses show N_4 values closer to the heavier analogues (LNBS to NBS, and RCBS to CBS), each have the higher T_g values.

Next, we look once more at the Raman spectra and obtain a glimpse into the intermediate range order dependence on alkali size. With the heavier alkali cations, M = Rb, Cs, 4-membered rings containing one $[B\emptyset_4]^-$ tetrahedron and three silicate tetrahedra (i.e., reedmergnerite rings), and/or 3-membered pure silicate rings are formed as evidenced by the ring breathing stretch at 595 cm^{-1}. Either one or both of these rings replace 4-membered rings with directly linked borate tetrahedra (i.e., danburite rings). The largest relative population of danburite rings is found for KBS (see Raman spectra in Fig. 15). The presence of danburite rings – while not necessarily representing the main structural unit of the KBS glass, still reflects on a very good mixing of silicate and borate units.

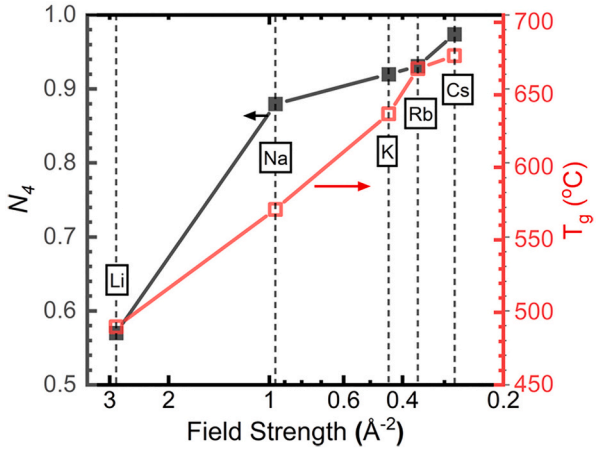

Fig. 19. Plot of the fraction of four-coordinated borate, N_4, (solid, black squares, left y-axis) and of the glass transition temperature, T_g, (open, red squares, right y-axis) versus the field strength of the alkali modifier for the MBS glasses ($16M_2O$-$10B_2O_3$–$74SiO_2$) of this study. Field strength values, calculated using effective ionic radius values from Shannon [8,45], are listed in Table 1. (For interpretation of the references to color in this figure legend, the reader is referred to the web version of this article.)

Interestingly, the maximum of mixed ring units coincides with the maximum in packing density that was found for this glass (see Fig. 5c).

Earlier studies by the authors on low alkali borosilicate glasses [1,11], challenged one hypothesis of the Yun-Dell-Bray model which suggested the preferential bonding of $[B\emptyset_4]^-$ to silicate tetrahedra [20,21]. In low alkali silicate glasses, Q^4 silicate tetrahedra prefer bonding to $B\emptyset_3$ over $[B\emptyset_4]^-$ units, whereas $[B\emptyset_4]^-$ favors bonds to other borate species. However, the current study supports the Yun-Dell-Bray model with good interlinking of $[B\emptyset_4]^-$ and silicate tetrahedra for this alkali rich glass system, and we can only speculate that the presence of non-bridging oxygen atoms on the silicate tetrahedra, even if a minority species, is one of the controlling differences.

Nickel confirms its role as a probe ion, changing its coordination and thus, the electronic transitions and color changes with the basicity of the glasses. The color change follows the average glass basicity, with high coordination and low valence for the low basicity LBS glass, despite the availability of sites with high micro-basicities provided by non-bridging oxygen in Q^2 and Q^3 units. The high basicity glasses KBS to CBS contain low coordinated Ni^{2+} and possibly Ni^{3+}. The optical spectra of NBS, despite the similar network as the heavier analogues and when considering merely the N_4 fraction and available nbO's for bonding, suggest low valent, high coordinated nickel. Small traces of trivalent nickel might be more prevalent in glasses than heretofore assumed.

4. Conclusions

The study of MBS glasses showed that LBS glass, with the Li-ion modifier of the highest field strength, exhibits visible phase separation while all other modifier cations give clear glasses after melt quenching and careful annealing from T_g. Small, clear LBS samples could be obtained by rapid quenching and analysis shows that Li_2O creates less borate tetrahedra, $N_4 \approx 0.57$, in quenched LBS compared to the annealed samples of the heavier alkali oxides with $N_4 \approx 0.88$ for NBS, increasing to $N_4 \approx 0.97$ for CBS. The remaining alkali oxides modify the silicate network by creating non-bridging oxygen in the form of Q^3 which for M = Na to Cs translates roughly into 20% Q^3 and 80% Q^4 groups. For quenched LBS, the observed modification of the silicate network is distinctly higher, and vibrational spectroscopy gives additional evidence for disproportionation of 2 Q^3 into Q^4 and Q^2 units, reflecting also on the higher fictive temperature of the quenched compared to annealed glasses. Compared to the other glasses, the high fraction of Q^4 silicate and $B\emptyset_3$ groupings might explain the resulting visible phase separation in the presence of the high field strength Li ions. In agreement with Sastry and Hummels [51] and in analogy to low alkali NBS glasses, we assume for LBS a silica rich matrix and a lithium borate rich spheres which contain $B\emptyset_3$, $[B\emptyset_4]Li$ and lithium modified silicate Q^2 and Q^3 units. Quenching from high temperature might further increase the high temperature species (trigonal borate, Q^2 Q^4 from disproportionation of Q^3 silicate) compared to annealed MBS samples. Quenching reduced the apparent separation into phases so that clear

samples were available for spectroscopic studies, but a high degree of preferential homonuclear bonding in the form of borate or silicate rings was found by vibrational as well as NMR spectroscopy. In glasses with M = Na to Cs, more cross linking between tetrahedral borate and silicate species is observed. The KBS glass showed the highest packing density, as well as the best mixing of the borate and silicate sub-networks as reflected by the highest contribution of danburite rings in the Raman spectra.

^{11}B NMR shows fewer B neighbors for each B_4 group for the heavier modifier containing glasses compared to those containing the lighter alkali ions. The B_4 shift is largest for LBS, the glass with the highest degree of preferential bonding (i.e., B-O-B) and as a result is prone to sub-liquidus phase separation. However, a more negative shift is observed for the B_4 resonances, even ever so slightly, from KBS to CBS. Here, ^{11}B NMR indicates more mixing between silicate and borate groups, consistent with Raman measurements that show more reed-mergnerite or 3-membered silica rings over danburite rings. Formations of rings without neighboring B_4 units might better accommodate larger modifier cations and account for the lower packing densities of RBS to CBS.

The transition temperature of the glasses increased with a higher N_4 and Q^4 fraction, which relates directly to a higher network connectivity as these glasses display four-fold instead of three-fold coordinated borate units, and at the same time have a less modified silicate network with more bridging oxygen atoms.

The probe ion nickel was present in LBS in its low basicity form, as divalent ions with a high coordination number, and did not reflect the higher micro-basicity sites of Q^2 ligands. As the average polarizability of the glasses increases, two more nickel species could be stabilized in glasses, e.g., tetrahedral Ni^{2+} and even trivalent nickel, a heretofore understudied species in glasses.

Declaration of Competing Interest

The authors declare that they have no known competing financial interests or personal relationships that could have appeared to influence the work reported in this paper.

Data availability

The authors confirm that the data supporting the findings of this study are available within the article.

Acknowledgements

We are grateful to Dr. Kim Tait, from the Royal Ontario Museum for providing the reference samples Danburite and Reedmergnerite.

Part of this material (Raman data) is based upon work supported by the National Science Foundation under Grant No. DMR-1626164.

The authors also thank Markus Seibt, Friedrich Alexander University Erlangen, Germany (Bachelor thesis 2018) and Amber Smith, Alfred University, Alfred, NY, USA (Bachelor thesis 2020) for their help in initial glass preparation and preliminary characterization.

Appendix A. Supplementary data

Supplementary data to this article can be found online at https://doi.org/10.1016/j.nocx.2023.100161.

References

[1] D. Möncke, G. Tricot, D. Ehrt, E.I. Kamitsos, Connectivity of borate and silicate groups in a low-alkali borosilicate glass by vibrational and 2D NMR spectroscopy, J. Chem. Technol. Metall. 50 (2015) 381–386.
[2] A. Winterstein-Beckmann, D. Möncke, D. Palles, E.I. Kamitsos, L. Wondraczek, A Raman-spectroscopic study of indentation-induced structural changes in technical alkali-borosilicate glasses with varying silicate network connectivity, J. Non-Cryst. Solids 405 (2014) 196–206.
[3] A. Winterstein-Beckmann, D. Möncke, D. Palles, E.I. Kamitsos, L. Wondraczek, Raman spectroscopic study of structural changes induced by micro-indentation in low alkali borosilicate glasses, J. Non-Cryst. Solids 401 (2014) 110–114.
[4] A.A. Osipov, L.M. Osipova, V.E. Eremyashev, Structure of alkali borosilicate glasses and melts according to Raman spectroscopy data, Glass. Phys. Chem. 39 (2013) 105–112.
[5] D. Manara, A. Grandjean, D.R. Neuville, Structure of borosilicate glasses and melts: a revision of the Yun, Bray and Dell model, J. Non-Cryst. Solids 355 (2009) 2528–2531.
[6] S. Bruns, T. Uesbeck, D. Weil, D. Möncke, L. van Wüllen, K. Durst, D. de Ligny, Influence of Al_2O_3 addition on structure and mechanical properties of borosilicate glassesInfluence of Al_2O_3 addition on structure and mechanical properties of borosilicate glasses, Front. Mater. 7 (2020) 189.
[7] O.V. Mazurin, Phase Separation in Glasses, North Holland, 1984.
[8] W. Vogel, Glass Chemistry, 2 ed., Springer-Verlag, 1994.
[9] V.J. Averjanov, O.W. Mazurin, J.A. Porai-Koschiz, H. Reiß, G.P. Roskova, W. Vogel, D. Ehrt, Influence of temperature on the conodes in phase separated glass melts of the system $BaO-B_2O_3-SiO_2$, Fiz. Chim. Stekla 5 (1979) 637–650.
[10] D. Möncke, D. Ehrt, H. Eckert, V. Mertens, Influence of melting and annealing conditions on the structure of borosilicate glasses, Phys. Chem. Glasses 44 (2003) 113–116.
[11] D. Möncke, G. Tricot, A. Winterstein-Beckmann, L. Wondraczek, E.I. Kamitsos, On the connectivity of borate tetrahedra in borate and borosilicate glasses, Phys. Chem. Glasses 56 (2015) 203–211.
[12] L.A. Bal'skaya, L.A. Grechanik, N.M. Vaisfel'd, Phase separation in low-alkali borosilicate glasses containing RO and Al_2O_3, in: E.A. Porai-Koshits (Ed.), Phase-Separation Phenomena in Glasses / Likvatsionnye Yavleniya v Steklakh / Ликвационные Явления в Стеклах, Springer US, 1973, pp. 107–113.
[13] L.-S. Du, J.F. Stebbins, Site connectivities in sodium aluminoborate glasses: multinuclear and multiple quantum NMR results, Solid State Nucl. Magn. Reson. 27 (2005) 37–49.
[14] D. Möncke, D. Ehrt, E.I. Kamitsos, Spectroscopic study of manganese-containing borate and borosilicate glasses: cluster formation and phase separation, Phys. Chem. Glasses Eur. J. Glass Sci. Technol. B 54 (2013) 42–51.
[15] E.I. Kamitsos, Infrared studies of borate glasses, Phys. Chem. Glasses 44 (2003) 79–87.
[16] A.C. Wright, The structural chemistry of B_2O_3, Phys. Chem. Glasses Eur. J. Glass Sci. Technol. B 59 (2018) 65–87.
[17] D. Möncke, E.I. Kamitsos, D. Palles, R. Limbach, A. Winterstein-Beckmann, T. Honma, Z. Yao, T. Rouxel, L. Wondraczek, Transition and post-transition metal ions in borate glasses: borate ligand speciation, cluster formation, and their effect on glass transition and mechanical properties, J. Chem. Phys. 145 (2016) 124501.
[18] D. Manara, A. Grandjean, N.D. R, Advances in understanding the structure of borosilicate glasses: A Raman spectroscopic study, Am. Mineral. 94 (2009) 777–784.
[19] B.C. Bunker, D.R. Tallant, R.J. Kirkpatrick, G.L. Turner, Multinuclear nuclear magnetic resonance and Raman investigation of sodium borosilicate glass structures, Phys. Chem. Glasses 31 (1990) 30–41.
[20] W.J. Dell, P.J. Bray, S.Z. Xiao, ^{11}B NMR studies and structural modeling of $Na_2O-B_2O_3-SiO_2$ glasses of high soda content, J. Non-Cryst. Solids 58 (1983) 1–16.
[21] Y.H. Yun, P.J. Bray, Nuclear magnetic resonance studies of the glasses in the system $Na_2O-B_2O_3-SiO_2$, J. Non-Cryst. Solids 27 (1978) 363–380.
[22] E. Stavrou, D. Palles, E.I. Kamitsos, A. Lipovskii, D. Tagantsev, Y. Svirko, S. Honkanen, Vibrational study of thermally ion-exchanged sodium aluminoborosilicate glasses, J. Non-Cryst. Solids 401 (2014) 232–236.
[23] F.L. Galeener, Planar rings in glasses, Solid State Commun. 44 (1982) 1037–1040.
[24] L.-S. Du, J.F. Stebbins, Solid-state NMR study of metastable immiscibility in alkali borosilicate glasses, J. Non-Cryst. Solids 315 (2003) 239–255.
[25] D. Möncke, E.I. Kamitsos, A. Herrmann, D. Ehrt, M. Friedrich, Bonding and ion-ion interactions of Mn^{2+} ions in fluoride-phosphate and boro-silicate glasses probed by EPR and fluorescence spectroscopy, J. Non-Cryst. Solids 357 (2011) 2542–2551.
[26] W.L. Konijnendijk, J.M. Stevels, The structure of borosilicate glasses studied by Raman scattering, J. Non-Cryst. Solids 20 (1976) 193–224.
[27] A. Herrmann, G. Völksch, D. Ehrt, Tb^{3+}as probe ion—clustering and phase separation in borate and borosilicate glasses, Int. J. Appl. Glas. Sci. 10 (2019) 532–545.
[28] D. Ehrt, H. Reiß, W. Vogel, Mikrostrukturuntersuchungen an CoO-haltigen $Na_2O-B_2O_3-SiO_2$-Gläsern, Silikattechnik 28 (1977) 359–364.
[29] M. Gitter, W. Vogel, Zur Farbe und Struktur ionengefärbter Gläser, Silikattechnik 29 (1978) 36–41.
[30] M. Gitter, W. Vogel, H. Schütz, Zur Kupfer (II)-, Nickel (II)-und Kobalt (II)-Koordination in Oxidgläsern, Wiss. Z. Friedrich-Schiller-Univ. Jena Math, 1983.
[31] M.D. Ingram, J.A. Duffy, Octahedral-tetrahedral transitions of cobalt(II) in sulphate-chloride glasses, J. Chem. Soc. A. Inorg. Phys. Theor. (1968) 2575–2578.
[32] J.A. Duffy, M.D. Ingram, A spectroscopic study of some transition-metal ions in acetic acid, in acetate glass and melt, and in nitrate glass, J. Chem. Soc. A. Inorg. Phys. Theor. (1969) 2398–2402.
[33] J.A. Duffy, Optical absorption of Na_2O-WO_3 glass containing transition-metal ions, J. Am. Ceram. Soc. 60 (1977) 440–443.
[34] R. Juza, H. Seidel, J. Tiedemann, Zur Kenntnis der Farbzentren in kobalt-, nickel-oder kupferhaltigen Alkaliboratgläsern, Angew. Chem. 78 (1966) 41–51.

[35] J. Matsuda, K. Kojima, H. Yano, H. Marusawa, Magnetic moments and ESR spectra of Co^{2+} ions in alkali borate glasses, J. Non-Cryst. Solids 111 (1989) 63–66.
[36] W. Weyl, Coloured Glasses, The Society of Glass Technology, Sheffield, 1951.
[37] T. Bates, Ligand field theory and absorption spectra of transition-metal ions in glasses, in: J.D. Mackenzie (Ed.), Modern Aspects of the Vitreous State, Butterworths, London, 1962, pp. 195–254.
[38] C.R. Bamford, Colour Generation and Control in Glass, Elsevier, 1977.
[39] C.R. Bamford, The application of the ligand field theory to coloured glasses, Phys. Chem. Glasses 3 (1962) 189–202.
[40] L. Galoisy, G. Calas, Role of alkali field strength on the speciation of Ni^{2+} in alkali borate glasses: comparison with crystalline Ni-borates, J. Non-Cryst. Solids 577 (2022) 121320.
[41] J.A. Duffy, Redox equilibria in glass, J. Non-Cryst. Solids 196 (1996) 45–50.
[42] A. Dietzel, M. Coenen, Über dreiwertiges Kobalt in Gläsern hohen Alkaligehaltes Glastechn. Ber. 34 (1961) 49–56.
[43] D. Möncke, D. Ehrt, Radiation-induced defects in CoO- and NiO-doped fluoride, phosphate, silicate and borosilicate glasses, Glas. Sci. Technol. 75 (2002) 243–253.
[44] D. Möncke, D. Ehrt, Irradiation induced defects in glasses resulting in the photoionization of polyvalent dopants, Opt. Mater. 25 (2004) 425–437.
[45] R.D. Shannon, Revised effective ionic radii and systematic studies of interatomic distances in halides and chalcogenides, Acta Cryst. A 32 (1976) 751–767.
[46] E.I. Kamitsos, Infrared spectroscopy of glasses, in: M. Affatigato (Ed.), Modern Glass Characterization, John Wiley & Sons, Inc, 2015, pp. 32–73.
[47] D. Massiot, F. Fayon, M. Capron, I. King, S. Le Calvé, B. Alonso, J.-O. Durand, B. Bujoli, Z. Gan, G. Hoatson, Modelling one- and two-dimensional solid-state NMR spectra, Magn. Reson. Chem. 40 (2002) 70–76.
[48] D. Massiot, C. Bessada, J.P. Coutures, F. Taulelle, A quantitative study of ^{27}Al MAS NMR in crystalline YAG, J. Magn. Reson. 90 (1990) 231–242.
[49] D. Möncke, Metal Ions and their Interactions in Covalent to Ionic Glass Systems - a Spectroscopic Study, Frierdich-Schiller-University Jena, 2017.
[50] J. Goldstein, A.D. Romig, D.E. Newbury, C.E. Lyman, P. Echlin, E. Lifshin, Image formation and interpretation, in: J. Goldstein, D.E. Newbury, D.C. Joy, C. E. Lyman, P. Echlin, E. Lifshin, L. Sawyer, J.R. Michael (Eds.), Scanning Electron Microscopy and X-Ray Microanalysis, Plenum Press, New York, NY, USA, 1992, pp. 191–198.
[51] B.S.R. Sastry, F.A. Hummel, Studies in lithium oxide systems: III, liquid immiscibility in the system Li_2O-B_2O_3-SiO_2, J. Am. Ceram. Soc. 42 (1959) 81–88.
[52] D. Ehrt, H. Reiß, W. Vogel, Einbau und Verteilung von Fe_2O_3 auf die Mikrophasen in Grundgläsern des Systems Na_2O-B_2O_3-SiO_2, Silikattechnik 27 (1976) 304–309.
[53] D. Möncke, G. Tricot, A. Winterstein, D. Ehrt, E.I. Kamitsos, Preferential bonding in low alkali borosilicate glasses, Phys. Chem. Glasses Eur. J. Glass Sci. Technol. B 58 (2017) 171–179.
[54] G.S. Henderson, The structure of silicate melts: a glass perspective, Can. Mineral. 43 (2005) 1921–1958.
[55] S. Kaneko, Y. Tokuda, Y. Takahashi, H. Masai, Y. Ueda, Structural analysis of mixed alkali borosilicate glasses containing Cs^+ and Na^+ using strong magnetic field magic angle spinning nuclear magnetic resonance, J. Asian Ceram. Soc. 5 (2017) 7–12.
[56] A. Vegiri, C.P.E. Varsamis, E.I. Kamitsos, Molecular dynamics investigation of mixed-alkali borate glasses: short-range order structure and alkali-ion environments, Phys. Rev. B 80 (2009).
[57] H. Uhlig, M.J. Hoffmann, H.-P. Lamparter, F. Aldinger, R. Bellissent, S. Steeb, Short-range and medium-range order in lithium silicate glasses, part I: diffraction exrperiments and results, J. Am. Ceram. Soc. 79 (1996) 2833–2838.
[58] J. Zhao, P.H. Gaskell, M.M. Cluckie, A.K. Soper, A neutron diffraction, isotopic substitution study of the structure of $Li_2O{\cdot}2SiO_2$ glass, J. Non-Cryst. Solids 232-234 (1998) 721–727.
[59] J. Swenson, L. Börjesson, W.S. Howells, Structure of borate glasses from neutron-diffraction experiments, Phys. Rev. B 52 (1995) 9310–9319.
[60] D.A. McKeown, G.A. Waychunas, G.E. Brown, EXAFS and XANES study of the local coordination environment of sodium in a series of silica-rich glasses and selected minerals within the Na_2O-Al_2O_3-SiO_2 system, J. Non-Cryst. Solids 74 (1985) 325–348.
[61] G. Greaves, Sodium environments in glass, J. Phys. Colloq. 42 (1981). C4-225-C224-228.
[62] O. Bouty, J.M. Delaye, S. Peuget, Europium structural effect on a borosilicate glass of nuclear interest, Proc. Chem. 7 (2012) 540–547.
[63] K. Handa, Y. Iwadate, N. Umesaki, Cation structure in binary potassium borate glasses, Jpn. J. Appl. Phys. 38 (1999) 140.
[64] W.E. Jackson, G.E. Brown, C.W. Ponader, X-ray absorption study of the potassium coordination environment in glasses from the $NaAlSi_3O_8$-$KAlSi_3O_8$ binary: structural implications for the mixed-alkali effect, J. Non-Cryst. Solids 93 (1987) 311–322.
[65] L. Cormier, P.H. Gaskell, G. Calas, A.K. Soper, Medium-range order around titanium in a silicate glass studied by neutron diffraction with isotopic substitution, Phys. Rev. B 58 (1998) 11322–11330.
[66] L. Cormier, G. Calas, B. Beuneu, Structure of single and mixed alkali li–Rb borate glasses by neutron diffraction, J. Non-Cryst. Solids 353 (2007) 1779–1784.
[67] S.V. Stefanovsky, J.J. Purans, Cesium speciation in nuclear waste glasses, Phys. Chem. Glasses Eur. J. Glass Sci. Technol. B 53 (2012) 186–190.
[68] P. Lv, C. Wang, B. Stevensson, Y. Yu, T. Wang, M. Edén, Impact of the cation field strength on physical properties and structures of alkali and alkaline-earth borosilicate glasses, Ceram. Int. 48 (2022) 18094–18107.
[69] Z.Y. Yao, D. Möncke, E.I. Kamitsos, P. Houizot, F. Célarié, T. Rouxel, L. Wondraczek, Structure and mechanical properties of copper–lead and copper–zinc borate glasses, J. Non-Cryst. Solids 435 (2016) 55–68.
[70] D. Ehrt, S. Flügel, Electrical conductivity and viscosity of phosphate glasses and melts, J. Non-Cryst. Solids 498 (2018) 461–469.
[71] F.V. Natrup, H. Bracht, Correlation between the cation radii and the glass transition in mixed cation silicate glasses, Phys. Chem. Glasses 46 (2005) 95–98.
[72] K. Griebenow, C.B. Bragatto, E.I. Kamitsos, L. Wondraczek, Mixed-modifier effect in alkaline earth metaphosphate glasses, J. Non-Cryst. Solids 481 (2018) 447–456.
[73] C.P. Rodriguez, J.S. McCloy, M.J. Schweiger, J.V. Crum, A.E. Winschell, Optical basicity and nepheline crystallization in high alumina glasses, in: Pacific Northwest National Laboratory Pacific Northwest National Laboratory, 2011.
[74] J.A. Duffy, The importance of π-bonding in glass chemistry: borate glasses, Phys. Chem. Glasses Eur. J. Glass Sci. Technol. B 49 (2008) 317–325.
[75] J.A. Duffy, A review of optical basicity and its applications to oxidic systems, Geochim. Cosmochim. Acta 57 (1993) 3961–3970.
[76] J.A. Duffy, Bonding, Energy Levels, & Bands in Inorganic Solids, Longman Group UK Ltd, 1990.
[77] V. Dimitrov, T. Komatsu, An interpretation of optical properties of oxides and oxide glasses in terms of the electronic ion polarizability and average single bond strength, J. Chem. Technol. Metall. 45 (2010) 219–250.
[78] T. Komatsu, V. Dimitrov, T. Tasheva, T. Honma, Electronic polarizability in silicate glasses by comparison of experimental and theoretical optical basicities, Int. J. Appl. Glas. Sci. 12 (2021) 424–442.
[79] J.A. Duffy, Optical basicity of fluorides and mixed oxide-fluoride glasses and melts, Phys. Chem. Glasses Eur. J. Glass Sci. Technol. B 52 (2011) 107–114.
[80] J.A. Duffy, M.D. Ingram, S. Fong, Effect of basicity on chemical bonding of metal ions in glass and its relevance to their stability, Phys. Chem. Chem. Phys. 2 (2000) 1829–1833.
[81] O. Schmitz-DuMont, H. Gössling, H. Brokopf, Farbe und Konstitution bei anorganischen Feststoffen. II. Die Lichtabsorption des zweiwertigen Nickels in oxydischen Koordinationsgittern, Z. Anorg. Allg. Chem. 300 (1959) 159–174.
[82] D. Möncke, D. Ehrt, Influence of melting and annealing conditions on the optical spectra of a borosilicate glass doped with CoO and NiO, Glas. Sci. Technol. 75 (2002) 163–173.
[83] J.A. Duffy, F.P. Glasser, M.D. Ingram, A spectrophotometric study of nickel(II) and cobalt(II) in sulphate-containing media, J. Chem. Soc. A. Inorg. Phys. Theor. (1968) 551–554.
[84] D. Möncke, D. Ehrt, Charge transfer transitions in glasses - attempt of a systematic review, Opt. Mater. X 12 (2021) 100092.
[85] M. Sanz-Ortiz, F. Rodríguez, J. Rodríguez, G. Demazeau, Optical and magnetic characterisation of Co^{3+} and Ni^{3+} in $LaAlO_3$: interplay between the spin state and Jahn–Teller effect, J. Phys. Condens. Matter 23 (2011) 415501.
[86] L. D'Amario, J. Föhlinger, G. Boschloo, L. Hammarström, Unveiling hole trapping and surface dynamics of NiO nanoparticles, Chem. Sci. 9 (2018) 223–230.
[87] L. D'Amario, R. Jiang, U.B. Cappel, E.A. Gibson, G. Boschloo, H. Rensmo, L. Sun, L. Hammarström, H. Tian, Chemical and physical reduction of high valence Ni states in mesoporous NiO film for solar cell application, ACS Appl. Mater. Interfaces 9 (2017) 33470–33477.
[88] N.V. Vasileva, P.A. Gerus, V.O. Sokolov, V.G. Plotnichenko, Optical absorption of Ni^{2+} and Ni^{3+} ions in gadolinium gallium garnet epitaxial films, J. Phys. D. Appl. Phys. 45 (2012) 485301.
[89] A. Davidson, J.F. Tempere, M. Che, H. Roulet, G. Dufour, Spectroscopic studies of nickel(II) and nickel(III) species generated upon thermal treatments of nickel/ceria-tupported materials, J. Phys. Chem. 100 (1996) 4919–4929.
[90] D. Möncke, M. Papageorgiou, A. Winterstein-Beckmann, N. Zacharias, Roman glasses coloured by dissolved transition metal ions: redox-reactions, optical spectroscopy and ligand field theory, J. Archaeol. Sci. 46 (2014) 23–36.
[91] H. Eckert, Structural characterization of noncrystalline solids and glasses using solid state NMR, Prog. Nucl. Magn. Reson. Spectrosc. 24 (1992) 159–293.
[92] D. Möncke, D. Ehrt, C.-P.E. Varsamis, E.I. Kamitsos, A.G. Kalampounias, Thermal history of a low alkali borosilicate glass probed by infrared and Raman spectroscopy, Glass Technol. Eur. J. Glass Sci. Technol. Part A 47 (2006) 133–137.
[93] G. Turner, K. Smith, R. Kirkpatrick, E. Oldfield, Boron-11 nuclear magnetic resonance spectroscopic study of borate and borosilicate minerals and a borosilicate glass, J. Magn. Reson. 67 (1986) 544–550.
[94] E.I. Kamitsos, A.P. Patsis, G. Kordas, Infrared-reflectance spectra of heat-treated sol-gel-derived silica, Phys. Rev. B 48 (1993) 12499–12505.
[95] T. Yano, N. Kunimine, S. Shibata, M. Yamane, Structural investigation of sodium borate glasses and melts by Raman spectroscopy. II. Conversion between BO_4 and BO_2O^- units at high temperature, J. Non-Cryst. Solids 321 (2003) 147–156.
[96] E.I. Morin, J. Wu, J.F. Stebbins, Modifier cation (Ba, Ca, La, Y) field strength effects on aluminum and boron coordination in aluminoborosilicate glasses: the roles of fictive temperature and boron content, Appl. Phys. A Mater. Sci. Process. 116 (2014) 479–490.
[97] P.M. Machowski, C.P.E. Varsamis, E.I. Kamitsos, Dependence of sodium borate glass structure on depth from the sample surface, J. Non-Cryst. Solids 345-346 (2004) 213–218.
[98] G. Lelong, L. Cormier, L. Hennet, F. Michel, J.-P. Rueff, J.M. Ablett, G. Monaco, Lithium borates from the glass to the melt: a temperature-induced structural transformation viewed from the boron and oxygen atoms, Inorg. Chem. 60 (2021) 798–806.

[99] L. Raffaëlly-Veslin, B. Champagnon, F. Lesage, Thermal history and manufacturing processes of Roman panes studied by Raman spectroscopy, J. Raman Spectrosc. 39 (2008) 1120–1124.
[100] L. Raffaëlly, B. Champagnon, N. Ollier, D. Foy, IR and Raman spectroscopies, a way to understand how the Roman window glasses were made? J. Non-Cryst. Solids 354 (2008) 780–786.
[101] E.I. Kamitsos, J.A. Kapoutsis, H. Jain, C.H. Hsieh, Vibrational study of the role of trivalent ions in sodium trisilicate glass, J. Non-Cryst. Solids 171 (1994) 31–45.
[102] E.I. Kamitsos, C.P.E. Varsamis, A. Vegiri, Spectroscopic studies of mobile cations in glass, Phys. Chem. Glasses Eur. J. Glass Sci. Technol. B 61 (2020) 107–122.
[103] E.I. Kamitsos, Y.D. Yiannopoulos, H. Jain, W.C. Huang, Far-infrared spectra of alkali germanate glasses and correlation with electrical conductivity, Phys. Rev. B 54 (1996) 9775–9783.
[104] E.I. Kamitsos, W.M. Risen, Vibrational-spectra of single and mixed alkali pentasilicate glasses, J. Non-Cryst. Solids 65 (1984) 333–354.
[105] A.C. Wright, Borate structures: crystalline and vitreous, Phys. Chem. Glass. Eur. J. Glass Sci. Technol. Part B 51 (2010) 1–39.
[106] F.L. Galeener, G. Lucovsky, J.C. Mikkelsen, Vibrational spectra and the structure of pure vitreous B_2O_3, Phys. Rev. B 22 (1980) 3983–3990.
[107] C.F. Windisch, W.M. Risen, Vibrational spectra of oxygen- and boron-isotopically substituted B_2O_3 glasses, J. Non-Cryst. Solids 48 (1982) 307–323.
[108] T. Furukawa, K.E. Fox, W.B. White, Raman spectroscopic investigation of the structure of silicate glasses. III. Raman intensities and structural units in sodium silicate glasses, J. Chem. Phys. 75 (1981) 3226–3237.
[109] G.D. Chryssikos, E.I. Kamitsos, A.P. Patsis, M.S. Bitsis, M.A. Karakassides, The devitrification of lithium metaborate: polymorphism and glass formation, J. Non-Cryst. Solids 126 (1990) 42–51.
[110] G.D. Chryssikos, E.I. Kamitsos, A.P. Patsis, M.A. Karakassides, On the structure of alkali borate glasses approaching the orthoborate composition, Mater. Sci. Eng. B 7 (1990) 1–4.
[111] G.N. Greaves, EXAFS and the structure of glass, J. Non-Cryst. Solids 71 (1985) 203–217.
[112] E.I. Kamitsos, G.D. Chryssikos, M.A. Karakassides, Glass transition phenomena and cation vibrations in alkali borate glasses, Phys. Chem. Glasses 29 (1988) 121–126.